Evolution of porewater composition through time in limestone aquifers: Salinity and D/H of fluid inclusion water in authigenic minerals (Jurassic of the eastern Paris basin, France)

Thomas Blaise, Alexandre Tarantola, Michel Cathelineau, Philippe Boulvais, Isabelle Techer, Thomas Rigaudier, Marie-Christine Boiron, Olivier Pierron, Philippe Landrein

Evolution of porewater composition through time in limestone aquifers: salinity and D/H of fluid inclusion water in authigenic minerals (Jurassic of the eastern Paris Basin, France)

Thomas BLAISE[1,2], Alexandre TARANTOLA[1,*], Michel CATHELINEAU[1], Philippe BOULVAIS[3], Isabelle TECHER[4], Thomas RIGAUDIER[5], Marie-Christine BOIRON[1], Olivier PIERRON[1] , Philippe LANDREIN[2]

[1] Université de Lorraine, CNRS, CREGU, GeoRessources, BP 70239, F-54506 Vandœuvre-lès-Nancy

[2] ANDRA, 1-7 rue Jean Monnet, F-92268 Châtenay-Malabry

[3] Géosciences Rennes, UMR 6118, Université Rennes 1 - CNRS, Campus de Beaulieu, F-35042 Rennes Cedex

[4] Université de Nîmes, EA 7352 CHROME, rue du Dr Georges Salan, 30021 Nîmes, FRANCE

[5] CRPG, 15 rue Notre Dame des Pauvres, F-54500 Vandoeuvre-lès-Nancy

* Corresponding author : Alexandre Tarantola, UMR GeoRessources 7539, Faculté des Sciences, Université de Lorraine, Boulevard des Aiguillettes, BP 70239, F-54506 Vandœuvre-lès-Nancy, France. e-mail : alexandre.tarantola@univ-lorraine.fr

Abstract

Past water circulations can significantly reduce the porosity and permeability of marine limestones. This is particularly the case in the Middle (Bathonian / Bajocian) to Upper (Oxfordian) Jurassic limestones from the eastern border of the Paris Basin. The knowledge of the timing, the temperature and composition of paleowaters is essential to model the hydrological evolution in this area where the Callovian-Oxfordian claystones are studied for the storage of nuclear wastes. In this way, fluid inclusions hosted in low-temperature (<60 °C) authigenic calcite, quartz and celestite crystals were analyzed by Raman spectroscopy and mass spectrometry to determine the chlorinity and D/H ratios. Chlorinity measurements (mmol Cl per liter of water) in fluid inclusions trapped in authigenic crystals during the late Jurassic / early Cretaceous period revealed unexpected high values, up to 3800 $mmol \cdot l^{-1}$, indicating that brines were involved in some of the diagenetic crystallization processes. By contrast, fluid inclusions in calcite cements of Cenozoic age within the Oxfordian limestones have low Cl concentration (less than 150 $mmol \cdot l^{-1}$), thus showing that a dilution event caused by water infiltrations during the Cretaceous uplift of this part of the basin has flushed out the original saline porewater. By coupling δD of fluid inclusion with $\delta^{18}O$ of calcite crystals, we estimate that calcite precipitation occurred at temperatures between 25 and 53 °C. The

hydrogen isotope composition of calcite-forming water is different between the Middle Jurassic (δD ranging from –20 to –35.8 ‰ $_{V\text{-}SMOW}$) and the overlying Oxfordian limestone (δD from –59.5 to –44.8 ‰ $_{V\text{-}SMOW}$). Present-day groundwaters are also of distinct composition on both sides of the Oxfordian claystones, indicating that limestone aquifers underwent independent hydrologic evolutions since the early diagenetic Jurassic cementation.

Keywords: Paris Basin, Jurassic, fluid inclusions, hydrogen stable isotopes, salinity, paleohydrology

Introduction

In the upper part of sedimentary basins, low-temperature diagenetic processes (<60 °C) may significantly modify the original porosity and permeability of the sediments through precipitation of authigenic cements. In such conditions, the chemical and isotopic composition of the fluids involved can be either characterized indirectly (*e.g.*, chemical and isotopic analyses of authigenic minerals) or directly through the study of fluid inclusions (e.g. Shepherd et al., 2000; Sandström and Tullborg, 2009; de Haller et al., 2011). The latter approach is somehow challenging in low-temperature systems. Indeed, fluid inclusions trapped at temperatures lower than ~ 50 °C are generally very scarce, metastable and composed of one phase (liquid) at room temperature (Goldstein, 2001), making impossible accurate microthermometric measurements (excepted by forcing the nucleation of a vapor phase, see Krüger et al., 2011). The evolution of the paleofluid chemistry from ancient hydrologic conditions up to present day is however of critical importance for the understanding of the regime of element mobility in modern aquifers (Hendry et al., 2015).

This is particularly the case for the aquifer-aquiclude system of the eastern part of the Paris basin, for which models of fluid circulation are needed. Indeed, since 1994, the French national radioactive waste management agency (Andra) has been studying the feasibility of a long-term geological disposal of intermediate to high level long-lived nuclear wastes. In this framework, an underground research laboratory (URL) was built in the East of the Paris Basin (Meuse/Haute-Marne) in a 150 m thick succession of Callovian - Oxfordian (COx) clay-rich rocks (present day depth between ~ 400 and 550 m). This formation is sandwiched between two limestone-dominated units: the overlying Oxfordian to Tithonian (Upper Jurassic) and the underlying Bathonian and Bajocian (Middle Jurassic) formations. Exchanges of gas and solutes through the Callovian-Oxfordian claystones occurred by diffusion (Lavastre et al., 2005), this process being responsible of the entire replacement of the original porewater at the Ma scale (Giannesini, 2006). Hence, the characterization of geological paleofluids related to the main fluid events helps understanding present poreawater composition.

Both Oxfordian and Middle Jurassic limestones have been intensively cemented by ancient water circulations (Clauer et al., 2007; Brigaud et al., 2010; Lavastre et al., 2011). With the exception of early cementation in phreatic or vadose environments, most of the porosity is filled by successive stages of calcite spars (Buschaert et al., 2004; Vincent et al., 2007; Brigaud et al., 2009a; Carpentier et al., 2014).

Analyses were performed during the past decade on calcite cements, particularly oxygen and carbon stable isotope data (Buschaert et al., 2004; Hibsch et al., 2005; Vincent et al., 2007; Brigaud et al., 2009a; Carpentier et al., 2014), strontium isotope data (Maes, 2002; Hibsch et al., 2005; Brigaud et al., 2009a), and Rare Earth Elements (Carpentier et al., 2014). These studies highlighted several stages of calcite cementation inferred to Early Cretaceous uplift

phases and Cenozoic tectonic stress periods. According to their $\delta^{18}O$ values and considering temperatures below 60 °C, Early Cretaceous calcite cements have likely originated from mixed marine and meteoric waters , whereas Cenozoic cementations are of meteoric origin (Buschaert et al., 2004; Brigaud et al., 2009a; Carpentier et al., 2014). Cenozoic cementation in the Oxfordian limestones filled most of the pore space and constitutes the only macroscopic crystals in geodes and vugs. Despite numerous available isotopic data on these cements, the precise origin of the calcite-forming water remains uncertain, as the temperature of crystallization derived from only six homogenization temperatures of primary fluid inclusions in calcite cements within the Oxfordian. Buschaert et al. (2004) estimated trapping temperatures between 32 and 42 °C after pressure correction.

Although somehow challenging, the measurements of fluid inclusion stable isotope compositions (δD and $\delta^{18}O$) might be of primary importance in the discussion of fluid-rock interactions (*e.g.*, Mazurek, 1999; Tarantola et al., 2007; Dublyansky and Spötl, 2010). However, with the exception of the preliminary study of Buschaert et al. (2004), no chemical and isotopic analyses of fluid inclusions were carried out and thus, the paleohydrological evolution of the studied area is still not fully understood (Dublyansky, 2004).

This paper presents a detailed investigation of fluid inclusions trapped in calcite, celestite and quartz cements in the Middle to Upper Jurassic limestones and marls formations in the eastern Paris Basin. It explores 1) how the analysis of fluid inclusions trapped in authigenic crystals provide information regarding the composition and temperatures of paleo-groundwaters in a low-buried sedimentary basin, and 2) how to reconstruct the timing and origin of fluid circulations in relation to regional geodynamic events from deposition time to present.

Geological setting

The intracratonic Meso-Cenozoïc Paris Basin was initiated after a general collapse of the Variscan massif during Permian times (*e.g.*, Mégnien et al., 1980). A westward shift of the subsidence towards the present day center of the Basin occurred during late Triassic (Carnian), which lead to the observed monocline structure. The eastern Paris Basin sedimentary formations gently dip to the West and show only local evidences of deformation.

Triassic sediments consist of fluvial siliciclastic deposits (Buntsandstein facies) grading into shallow-water marine carbonates (Muschelkalk facies) and evaporites (Keuper facies). The Lower Jurassic sedimentary formations consist mainly of marls and shales deposited during the Carnian to Toarcian stratigraphic cycle (Guillocheau et al., 2000). This period corresponds to a large opening of the Basin and to a transgression of the Tethys sea from the East. The early Bajocian marked the transition to a vast carbonate environment (Durlet and Thierry, 2000), with the deposition of oobioclastic sediments together with coral buildups. A major change of facies occurred at the early / late Bajocian transition, with mixed carbonate (ooid-dominated) and siliciclastic sedimentation (Brigaud et al., 2009b). A new carbonate ramp then developed in the northeastern Paris Basin during the Bathonian, with typical inner ramp depositional environment (oolitic shoal or lagoon). A general drowning of the platform resulting in deposition of clay-rich sediments started during the Callovian and lasted until the early Oxfordian. The depositional environment gradually returned to carbonate sedimentation during the Middle Oxfordian, with reefal-dominated and oolitic limestones. Lowstand relative sea-level favored the increase of siliciclastic inputs at the beginning of the late Oxfordian (Carpentier et al., 2010). A major carbonate crisis occurred at the Oxfordian/Kimmeridgian transition (Lefort et al., 2011), with marl dominated

sedimentation, coming next with a mixed carbonate and siliciclastic ramp environment during the Tithonian. During late Cimmerian and late Aptian, two stages of emersion associated with erosion occurred (Quesnel, 2003), as a result of both eustatic sea-level drop and distant influence of uplift of rift shoulder linked to the North Atlantic rifting (Ziegler, 1990). A large transgression occurred in late Cretaceous times resulting in the deposition of chalk. The eastern basin margin definitively emerged and experienced weathering and erosion during the Cenozoic, allowing the exhumation of the underlying Jurassic and Triassic sediments, which presently crop out in the area.

The tectonic agenda in this part of the Basin was summarized by André et al. (2010). Two main stages have been distinguished:

i) Early stages, as recorded by the formation of discrete clay minerals (I/S minerals dated around 150 ± 10 Ma (Rousset and Clauer, 2003). Several episodes of thermal anomalies linked to the rifting of the central Atlantic Ocean are well known in Western Europe. Major hydrothermal events occurred during the Jurassic (190-170 Ma and ~ 150 Ma) resulting in Pb-Zn-Ba-F and U mineralizations along the margins of the basin, and in the Armorican, Central and Morvan massifs (Lancelot et al., 1984; Bonhomme et al., 1987; Respaut et al., 1991; Cathelineau et al., 2004, 2012), as well as widespread illitization in Permian and Triassic sandstones (Clauer et al., 1995). Other major extensional events favoring fluid circulations are known at ~ 120 Ma and 80 Ma (Clauer et al., 1995, 1996). All these events coincide with an increase in the subsidence rate in the Paris Basin (Ferry et al., 2007).

ii) Main tectonic events occurred during the Cenozoic, as the basin was submitted to the Pyrenean and Alpine orogenies, as well as extensional movements symmetric and synchronous of the continental rifting of the Rhine graben, such as the Gondrecourt graben delimiting the URL area (Fig. 1). Major faults, inherited from the Hercynian orogeny may also have been active during the Mesozoic and then reactivated by the Pyrenean and Alpine events (André et al., 2010).

The geothermal gradient in the URL area is around 3 °C / 100 m (Landrein et al., 2013). The burial and thermal history of the Mesozoic series was reconstructed by the study of several independent geothermometers (Blaise et al., 2014). Maximum burial temperatures, reached during the Late Cretaceous, were estimated of 40 ± 5 °C in the Upper Oxfordian and 60 ± 5 °C in the Middle Jurassic limestones (Fig. 2).

Sampling

Core samples

The macroscopic evidences of water-rock interactions during burial diagenesis and telogenesis are the diagenetic/hydrothermal cements that may fill the porous space in limestones located on both sides of the Callovian-Oxfordian claystones. These evidences are scarce, but vugs and geodes were found at the base of the Oxfordian limestones, and within the Bajocian formation. Samples have been recovered thanks to five drill cores cutting through all the series near the URL site (Fig. 1). Seven samples hosting vugs were selected for D/H analysis of water trapped within fluid inclusions (four in the Oxfordian and three in the Middle Jurassic limestones, Fig. 1, Table 1). Samples consist of euhedral calcite, either scalenohedral or globular, found in vugs originating from bioherm units, and of quartz-celestite assemblage found in cavities originating from the dissolution of bioclasts and compaction cracks in the *Terrain à Chailles*, at the top of the Callovian-Oxfordian claystones. According to U-Pb dating, authigenic calcite crystallized at two distinct periods (Pisapia et al.,

2011): 149.2 ± 5.8 Ma in the Middle Jurassic limestones (*i.e.*, during the late Jurassic / early Cretaceous period) and 33.2 ± 5.5 Ma in the Oxfordian (*i.e.*, during the late Eocene – Oligocene period). The authigenic calcite found in the Dogger samples corresponds to the "Bc1" or "Bc2" stages described by Brigaud et al. (2009a), (named "Cal1" and "Cal2" in Carpentier et al., 2014). The samples selected for D/H measurements were also prepared for fluid inclusion petrography and salinity measurements (Table 1). Four other samples were investigated for the measurement of the salinity of water of fluid inclusions by Raman spectroscopy in quartz (one sample in the Lower Oxfordian) and celestite (three samples in the Middle Oxfordian, Lower Oxfordian and Bathonian) (Table 1). Other core samples from Lower Oxfordian to Bathonian series were selected for mineral isotopic analyses (O, C, Sr) (Table 2). As sampling was carried out from five different wells in the Andra studied area, the depth of each sample is normalized to the depth measured in the borehole HTM102 (Fig. 1D).

Outcrop samples

Seven outcrop samples have been selected (Fig. 1, Table 1): five fracture-filling calcite grains in hydrothermal breccias formed during the Oligocene, crosscutting the Upper Oxfordian to Lower Kimmeridgian limestones, at the eastern flank of the Gondrecourt graben (Augeville), one fracture-filling calcite, also formed during the Oligocene, within the Upper Oxfordian limestones near Leurville and one vug-filling calcite in the Bajocian limestones sampled at the Sommerécourt quarry, close to the "Vittel fault".

Analytical procedures

1. Petrography

Conventional 30 µm thin sections were prepared for each sample for petrographic observations. All samples were observed by cathodoluminescence, with a 8200 CCl CITL apparatus, coupled with an Olympus microscope provided with an AxioCam digital camera (*GeoRessources* laboratory, Nancy, France). In order to provide complementary information on calcite composition, some thin sections were stained after reaction with an alizarin-potassium ferricyanide solution. Fluid inclusion petrography and Raman spectroscopy analyses were carried out from double-polished thick sections (200 – 300 µm).

2. Raman spectroscopy

Fluid inclusions in quartz, celestite, and calcite were investigated with a LabRAM HR Raman spectrometer for gas and chlorinity (chloride concentration) determination, using a monochromatic beam at 457 nm, at the *GeoRessources* laboratory (Nancy, France). In calcite, the efficiency of this method can be limited by several factors, including (1) the size and shape of fluid inclusions (predominantly < 5 µm and flat shaped), (2) high birefringence of calcite and (3) fluorescence of the mineral matrix. The latter parameter strongly depends on the amount of Fe^{2+} in calcite. Indeed, ferroan calcite usually shows some fluorescence, which may prevent any spectroscopic characterization of the fluid phase. Fluid inclusion chlorinity was obtained from the stretching band of water at mineral optical extinction, following the methodology described in Dubessy et al. (2002), Baumgartner and Bakker

(2008), Caumon et al. (2013, 2015) and Tarantola and Caumon (2015). Results are given in $mmol \cdot l^{-1}$ with an accuracy of ± 10 %.

3. Isotopic measurements

The hydrogen and oxygen isotopic signatures (δD and $\delta^{18}O$) of paleowaters trapped within fluid inclusions are obtained by two different ways. The δD value is obtained by direct analysis of the water after extraction from the host-mineral. Because we are dealing with primary fluid inclusions, calcite, celestite and quartz precipitated from the circulating fluid. The $\delta^{18}O$ value of the paleofluid is obtained from the oxygen isotopic value of the host-mineral after equilibrium fractionation calculation at selected temperatures.

Hydrogen isotopes

Calcite and celestite crystals were weighted (1.0 to 8.2 g, Table 1) and introduced into steel tubes. Calcite-bearing tubes were connected to a vacuum extraction line and heated overnight at 120 °C to release H_2O molecules adsorbed at the mineral surface (Dublyansky and Spötl, 2009). Preliminary tests conducted under the microthermometric heating stage had shown that our fluid inclusions did not decrepitate, nor stretch, for temperatures below 200 °C. The calcite-bearing tubes were subsequently crushed under vacuum to release all fluids hosted in crystals. H_2O (and possibly CO_2) were trapped under vacuum in a liquid nitrogen-cooled U-shaped tube, incondensable gases being directly removed from the extraction line. CO_2 was never found in sufficient amount to be analyzed, and was thus removed from the line. H_2O was reduced into H_2 by passing through a uranium reactor heated at 800 °C. H_2 was trapped in glass tubes and analyzed using a VG 602D mass spectrometer at *CRPG* laboratory (Nancy, France). All results are expressed with respect to V-SMOW. Two in-house standards were weekly extracted and analyzed to optimize the accuracy of the isotopic measurements.
An advantage of the metal reduction method for the preparation of gas sample for hydrogen isotope ratio analysis is the small size of the sample < 1 µl (Wong et al., 1984). Water is reduced into H_2 by passing through a uranium reactor heated at 800 °C (Bigeleisen et al., 1952). The same reagent is used for the reduction of consecutive water samples. Because water adheres to the internal surfaces of the vacuum system, D/H isotope analysis experiences a memory effect, where the measured D/H ratio of a sample is displaced, from its true value, towards the D/H ratio of the previous samples. Memory effects are most pronounced when consecutive samples have substantially different isotopic compositions as well as when the amount of water reduced in the reactor is significantly different. To avoid this issue, samples were systematically duplicated, and the δD deviance between each isotopic measurement was less than ± 1.5 ‰. For each duplicate, δD values from the first extraction were thus not considered, as potentially affected by this memory effect. Taking into account the overall reproducibility of internal standards and sample duplicates, the accuracy of D/H measurements is lower than 3 ‰.

C and O stable isotopes

Calcite spars, quartz and amorphous silica were extracted from fractures and vugs and picked out under the microscope to select monogenic crystals. The finely crushed carbonate and silicate materials were reacted respectively, with anhydrous H_3PO_4 at 50 °C during 15

hours and with BrF_5 in Ni tubes at 670 °C overnight (following the method of Clayton and Mayeda, 1963). After silicate dissolution, the liberated O_2 was converted into CO_2 by reaction with hot graphite. Isotopic analyses were carried out on CO_2 gas using a VG SIRA 10 mass spectrometer at *Geosciences Rennes* laboratory (France) and expressed with the conventional delta notation vs. V-SMOW (O) and PDB (C). Analytical precision was quantified at ± 0.1 ‰ for both C and O, using in-house carbonate standard *Prolabo Rennes* and NBS 19 reference material.

Sr isotopes

Picked celestite crystals were partially dissolved in HNO_3. Separation of Sr for isotopic determination was conducted on a Sr-resin, following the methodology described by Pin et al. (2003). Leachates were evaporated, redissolved in HNO_3 and deposited on Ta filaments. Rb and Sr isotopes were measured on a Triton TI TIMS at *GIS laboratory* (Nîmes, France). Values are reported as $^{87}Sr/^{86}Sr$ ratios. The external reproducibility of the isotopic measurements was controlled by periodic analysis of the NBS 987 standard providing a mean $^{87}Sr/^{86}Sr$ ratio of 0.710258 ± 2.10^{-6} (2σ). The $^{87}Sr/^{86}Sr$ ratios were measured at least 90 times to ensure an analytical error below 5.10^{-6} (2σ).

Results

1. Petrographic description

Crystallization of authigenic minerals can be macroscopically observed within vugs and compaction cracks (Fig. 3a, b). Euhedral sparite fringe formed at the border of the micritic matrix (“Spar 1”, Fig. 3c, d, e, f). Their coloration by reaction with an alizarin solution revealed a clear gradation in composition, with an increase of the Fe/Mg ratio towards the edge of the crystals (Fig. 3f). They are followed by amorphous silica, which forms spherulites or irregular fringes (Fig. 3c-h), sometimes crosscutting calcite spars (Fig. 3f). Quartz postdates chalcedony and occurs either as microcrystalline fringe (Fig. 3c, d) or euhedral crystals (Fig. 3f, g). The remaining space is filled by celestite (Fig. 3c, d, f) or sparite (Fig. 3e). The second stage of sparite (“Spar 2”) crosscuts, and thus postdates, celestite infillings (Fig. 3h). A detailed petrographic description of the calcite samples can be found in Carpentier et al. (2014) and reference therein.

2. O, C and Sr isotopes

O and C stable isotope measurements were carried out for calcite samples, O stable isotopes for quartz and amorphous silica and Sr stable and radiogenic isotopes for celestite crystals. All results are presented in Tables 1 and 2. The O isotope composition ($\delta^{18}O$) of calcite from the vugs is between 21.4 and 24.2‰ and between 20.7 and 21.9‰ for the hydraulic breccias of the Upper Oxfordian (locality of Augeville and Leurville). All $\delta^{13}C$ values are positive, between 0.0 and +3.1‰. In the boreholes (Table 2), the calcite spar has comparable $\delta^{18}O$ and $\delta^{13}C$ values of 21.2 and +1.5‰, respectively. Quartz and chalcedony have $\delta^{18}O$ values of 33.2 and 32.4‰, slightly above the calcite value of the host marl ($\delta^{18}O$ = 30.0‰).

3. Fluid inclusions

Petrography

As mechanical crushing of crystals releases the bulk fluid content trapped within the inclusions, careful petrography was carried out on fluid inclusions in calcite crystals (Fig. 4). Fluid inclusions are typically of small size (< 5 µm) and exhibit a single metastable aqueous liquid phase at room temperature (Fig. 4a, b), which prevents the determination of fluid salinity and minimal trapping temperatures by standard microthermometric methods. No nucleation of a vapor phase occurred within the inclusion after successive cycles of freezing and melting. In calcite, the discrimination between the primary or secondary origin of fluid inclusion cannot always be achieved as both may be aligned along the cleavage planes of the crystals. When fluid inclusion planes are restricted to a single crystal (as illustrated on Fig. 4c), the inclusions can be interpreted either as primary or as pseudo-secondary (Goldstein and Reynolds, 1994). However, this petrographic criteria may be lacking, so the origin of the inclusions remains unclear (Fig. 4b, d). It is worth noting that no clear secondary fluid inclusion planes, crosscutting several crystals, were observed. As a result, the fluid observed in the crystals is assumed to be the fluid present during crystal growth.

Fluid inclusion composition

Raman spectroscopy was performed on the aqueous phase only. Most of the fluid inclusions are free of volatile species with the exception of small amounts of CH_4 and CO_2 rarely detected.

The deformation of the stretching band of water can be assigned to increasing chlorinity values (Dubessy et al., 2002; Baumgartner and Bakker, 2008; Caumon et al., 2013, 2015). Tarantola and Caumon (2015) observed a slight effect of metastability (metastable one-phase (L) versus stable two-phase (LV)) increasing with the degree of metastability of the inclusion. According to the estimated trapping conditions at temperatures lower than 60 °C in the H_2O-NaCl system, the negative pressure prevailing within fluid inclusions should lie in the range 70-100 MPa at Raman spectroscopy measurement conditions (20 °C). In this case, metastable fluid inclusions record a salinity overestimated of maximum 5 to 8 relative mass% NaCl compared to what would be measured in a stable two-phase fluid inclusion (Tarantola and Caumon, 2015).

Both core and outcrop samples of authigenic calcite within the Oxfordian limestones, as well as samples from the Bajocian quarry at Sommerécourt, are characterized by low to non-saline fluid inclusions (Cl concentration between 0 and 160 $mmol \cdot l^{-1}$, Table 1). By contrast, vug-infillings calcite from the Middle Jurassic core samples contains a much more saline fluid. These brines have a chlorine concentration ranging from 650 to 2700 $mmol \cdot l^{-1}$. Such values are significantly higher than the average present-day seawater (~ 550 $mmol \cdot l^{-1}$, Fontes and Matray, 1993a). Fluid inclusions hosted in quartz and celestite crystals in the Middle to Lower Oxfordian limestones display chlorine concentrations ranging from 320 to 3660 $mmol \cdot l^{-1}$ (Table 1). In the Bathonian, vug-filling celestite crystals contain fluid inclusions also with a large range of chlorinity values, between 760 and 3840 $mmol \cdot l^{-1}$.

δD of fluid inclusions

Core samples

The hydrogen isotope ratio, expressed as δD, of the water trapped in fluid inclusions within authigenic calcite crystals range between –20 and –60 ‰ (Table 1). In the Oxfordian limestones, the δD values of calcite inclusion-water range between –45 and –60 ‰. In the Middle Jurassic limestones, inclusion water shows by contrast higher δD between –20 and –36 ‰. The hydrogen isotope value of the water trapped in fluid inclusions within celestite is –94 ‰ (Table 1).

Outcrop samples

Hydrothermal breccias formed during the Cenozoic have been sampled in Augeville and Leurville (Fig. 1). They contain numerous fluid inclusion and yield δD values ranging from –40 to –54 ‰ (Table 1). Fluid inclusions trapped in vug-filling calcite in Middle Jurassic limestones from Sommerécourt have comparable δD values: two values were obtained, yielding δD of –48 and –51 ‰.

Discussion

1. Chalcedony-quartz-celestite assemblage as a record of the evolution of porewater composition

The chalcedony-quartz-celestite succession, infilling moldic porosity and compaction cracks are essentially found in the *Terrain à Chailles* silty-marl layer. This formation, usually characterized by its abundant chert nodules, is situated at a lithologic transition between the Callovian-Oxfordian claystones (COx) and the Oxfordian limestone aquifer. In minor amounts, silica and celestite are also found as diagenetic phases within the COx itself (Lerouge et al., 2011), and a single occurrence of celestite has been detected in the underlying Bathonian limestones (this study). The chalcedony-quartz-celestite succession is sometimes predated by pyrite, dolomite and siderite, interpreted as early diagenetic on the basis of petrographic criteria and geochemical analyses (Lerouge et al., 2011). However, no explanation has been so far advanced for the origin of siliceous cements and their specific occurrence at the top of the COx formation. The *Terrain à Chailles* is overlaid by another marly formation, the *Marnes des Eparges,* with a decametric spongolite facies. In this layer, abundant sponge spicules are recrystallized in calcite. The dissolution of biogenic silica is common during early diagenesis (Hendry and Trewin, 1995; DeMaster, 2004; Madsen et al., 2010), SiO_2 being transported in solution and further crystallized as amorphous silica (chalcedony) and quartz. The transition from the amorphous polymorph to euhedral quartz can be gradual (Fig. 3a, b), and is rather due to relative rates of nucleation and growth than the result of a temperature increase (Williams et al., 1985). Using the fractionation coefficient of Kita et al. (1985) between amorphous silica and H_2O, the calculated $\delta^{18}O$ of parent-water ranges between –1.5 and +0.9 ‰, at 30 and 40 °C, respectively. Within the same temperature conditions, $\delta^{18}O$ of water involved in quartz crystallization ranges from –1.5 and +1.1 ‰ (Zheng, 1993). These ranges match the seawater domain (Fig. 5). The very D-depleted water trapped within fluid inclusion of celestite samples possibly records the involvement of biogenic methane during early diagenetic processes. Indeed, methane, either of biogenic or thermogenic origin, is strongly depleted in D (Schoell, 1980). Fluid inclusions with δD ranging from –40 to –110 ‰ have already been documented in various minerals

(calcite, quartz, fluorine, and galena) crystallized at temperatures of 70 to 150 °C, and interpreted as a possible interaction with organic fluids (Charef and Sheppard, 1987; Munoz et al., 1999; Tarantola et al., 2007).

The precipitation of sulfate minerals (gypsum or anhydrite) prior the chalcedony stage is suggested by the preservation of lamellar crystal pseudomorphs (Fig. 3c). Dissolved gypsum or anhydrite associated with chalcedony has been reported in several studies, either in geodes (Boyce et al., 1990; Chowns and Elkins, 1974; Gomez-Alday et al., 2002), evaporitic beds and nodules (Milliken, 1979; Ulmer-Scholle et al., 1993) or cherts (Chowns and Elkins, 1974; Folk and Pittman, 1971; Geeslin and Chafetz, 1982). The precipitation of gypsum or anhydrite likely occurred from sulfate-rich dense brines (Hanor, 2004) percolating downwards, from the surface down to the permeability transition between claystones and limestones. Regarding the large amount of Sr needed to crystallize celestite, the most likely reservoir is coral aragonite (Finch and Allison, 2003), Sr being released during the recrystallization of aragonite into calcite (Baker and Bloomer, 1988; Hoareau et al., 2010). Corals build-up consistently forms several decametric levels within the Middle and Upper Oxfordian limestone units.

The contribution of brines is supported by chlorine concentration of fluid inclusion in quartz and celestite, ranging from 320 to 3620 $mmol \cdot l^{-1}$, and from 850 to 3690 $mmol \cdot l^{-1}$, respectively (Table 1). This brine was likely generated by the evaporation of seawater beyond gypsum saturation. The large range of chlorinity provides evidence of a mixing trend between this evaporitic end-member, which has been more or less diluted by seawater and/or meteoric water. Additionally, it is known that Sr concentration in water increases significantly with salinity (Hanor, 2000; 2004). A contribution of secondary brines from the dissolution of Upper Triassic halite is unlikely, regarding $^{87}Sr/^{86}Sr$ values of celestite close to Upper Jurassic seawater (Jones et al., 1994), excepting a single value (sample PPA- 360 m, $^{87}Sr/^{86}Sr$ = 0.707545, Table 2). A contribution of ascending Triassic fluids would increase the $^{87}Sr/^{86}Sr$ ratio, from the dissolution of halite and the interaction with siliciclastic series. Late calcite, postdating quartz (Fig. 3g) and celestite (Fig. 3h), has a $\delta^{18}O$ value of 21.2 ‰. Considering a range of crystallization temperature between 30 and 40 °C (Blaise et al., 2014), $\delta^{18}O$ of parent-water is between –8.8 and –6.5 ‰ (Zheng, 1999), indicating a meteoric origin. Therefore, the chalcedony-quartz-celestite-calcite assemblage provides a unique record of the transition in the composition of porewater, from the concentration of seawater by evaporation to the meteoric water infiltration (Fig. 5).

According to the geodynamical evolution of the basin, meteoric water recharge could have started since early Cretaceous. Thermal anomalies linked to the opening of the central Atlantic Ocean engendered the general emersion of the north-eastern flank of the Paris Basin at the end of Jurassic (during the “Late Cimmerian Unconformity”, LCU). The sea regression is marked by a sabkha environment, with dolomite and anhydrite precipitation during the late Tithonian (“Purbeckian” facies, Guillocheau et al., 2000). At that time evaporated seawater could have migrated downwards due to its higher density, towards the permeability transition between claystones and limestones; alternatively, lateral migration from the north-eastern border of the basin could be invoked. These brines were involved in the precipitation of silica (chalcedony and quartz) and sulfates (celestite and possibly gypsum/anhydrite), before being progressively flushed out by the percolation of fresh meteoric water during the Cretaceous period. Mixing between seawater and meteoric water could also have induced calcite precipitation in the Middle Jurassic aquifer.

2. Comparison with present-day groundwaters

Hydrogeochemistry of present-day underground waters

The chemical and isotopic signatures of present-day groundwater percolating through the porous levels of Oxfordian and Middle Jurassic limestones have been extensively monitored in and around the Andra studied area (Buschaert et al., 2007; Linard et al., 2011; Rebeix et al., 2011). The stable isotope (δD and $\delta^{18}O$) composition of water reveals a strictly meteoric signature (Gianessini, 2006; Linard et al., 2011; Rebeix et al., 2011). Water residence time was estimated on the basis of geochemical tracers to be of about 10 ka for the Oxfordian aquifer and several hundred thousand years in the Middle Jurassic. This implies a recharge of the aquifers under different paleoclimatic conditions. The extremely low-permeable Callovian-Oxfordian claystones prevent any connection between the aquifers that, as a result, should be considered as isolated hydrological systems (Lavastre et al., 2010). However, chemical exchanges of gas and solutes through the Callovian-Oxfordian claystones occur by diffusion (Lavastre et al., 2005; Battani et al., 2011; Bensenouci et al., 2013; Fourré et al., 2011; Mazurek et al., 2011; Rebeix et al., 2011), this process being responsible of the entire replacement of the original Callovian-Oxfordian porewater (Giannesini, 2006).
The thick Lower Jurassic clay-rich sediments, together with the Keuper halite, constitute an efficient isolation between the Middle Jurassic limestones and the deep siliciclastic Lower Triassic aquifer (Marty et al., 2003). Chlorine concentration and $\delta^{37}Cl$ evolution with depth can be interpreted as the result of diffusive transfers from the Keuper halite through the entire Jurassic sedimentary sequence. Such a process may explain chlorine concentrations in the present-day groundwaters (Rebeix et al., 2011).
Towards the central part of the basin, the deep Middle Jurassic and Triassic groundwaters have significant different chemical compositions. Their salinity gradually increases from fresh or brackish waters to brines in the deepest part of the basin (Fontes and Matray, 1993b; Matray et al., 1994; Pinti et al., 1997; Worden et al., 1999; Millot et al., 2011), as a result of a complex mixing process between both primary and secondary brines together with dilution related to meteoric water inputs (Matray and Fontes, 1990). In addition, cross-formational flow from the Triassic sandstones to the Middle Jurassic limestones may have occurred through the fracture network (Worden and Matray, 1995).

Stable isotope signature of paleowaters

As discussed above, petrographic criteria were not always clear enough to determine accurately the relative age of fluid inclusions trapped in calcite crystals. However, a large majority of fluid inclusions is likely of primary origin, and no clear secondary fluid inclusion planes were identified. Therefore, bulk fluid δD values can be considered as representative of the water involved in calcite precipitation. Previous published studies on δD measurements from fluid inclusions hosted in low-temperature calcite have shown that they preserve the original isotopic composition of the forming waters (McGarry et al., 2004; Zhang et al., 2008; Dublyansky and Spötl, 2009, 2010)
The δD value of water trapped in fluid inclusions is reported as a function of the $\delta^{18}O$ values of calcite parent-fluids in Figure 6. The oxygen isotope equilibrium fractionation between calcite and water ($\Delta^{18}O_{Cal\text{-}H2O}$ = 28.8‰) was calculated considering a mean crystallization temperature of 35 °C, and using the calcite-water fractionation factor of Zheng (1999). The value of 35 °C is used here to normalize all samples and be able to visualize them in a δD vs.

$\delta^{18}O$ plot. This temperature is close to those calculated from fluid inclusion homogenisation temperatures in authigenic calcite in the Oxfordian limestones (Buschaert et al., 2004), but also to the first and second generation of calcite in the Middle Jurassic limestones (Brigaud et al., 2009a).

With the exception of the Middle Jurassic sample 481 m, the isotopic composition of calcite-forming water plots close to the Global Meteoric Water Line (GMWL, Craig, 1961). This illustrates the predominance of meteoric water within the aquifers. As illustrated on Fig. 6, a crystallization temperature of 35 °C leads to a shift of the isotopic composition of some Oxfordian paleowaters (samples 569 m, 660 m, 134 m and 340 m) to the right of the GMWL. This is likely due to an overestimation of the temperature, which should thus be below 35 °C (Fig. 6). Several other processes may also account for the modification of the isotopic composition of meteoric water, among which (1) subsurface evaporation (*e.g.*, Gonfiantini, 1986; Gibson et al., 1993), (2) ^{18}O-enrichment by fluid-rock interactions (*e.g.*, Sheppard, 1986; Matray and Fontes, 1990; Kharaka and Thordsen, 1992) or (3) mixing with other fluids, including seawater (*e.g.*, Lynn Ingram et al., 1996):

(1) Subsurface evaporation leads to the enrichment of the residual water in both ^{18}O and D. However, the mass of evaporated meteoric water isotopically enriched by evaporation is usually limited and tends to be highly diluted by fresh water as it reaches the saturated zone (IAEA, 2000a; 2000b). Present-day groundwaters flowing through the Jurassic aquifers in the eastern or central part of the Paris Basin are for example not significantly affected by evaporation (Matray et al., 1994; Rebeix et al., 2011).

(2) Isotopic exchange reactions between groundwater and carbonates are well documented (Kharaka and Carothers, 1986). In both studied limestone units, the $\delta^{13}C$ values of calcite are similar to those of host limestones, suggesting that carbon in the newly-formed calcite was supplied by the dissolution-precipitation processes with the host rock (Buschaert et al., 2004; André et al., 2010). Buffering of pore water by carbonate dissolution may also increase its original ^{18}O content (*e.g.*, Clayton et al., 1966).

(3) Significant interaction of calcite-forming waters with liquid or gaseous hydrocarbons can be discarded. No hydrocarbon accumulations have been evidenced within the Jurassic sediments in the eastern part of the Basin because the too low temperatures reached by hydrocarbon source rocks prevented any oil formation (Blaise et al., 2011; 2014). Furthermore, fluid inclusions in calcite are all one-phase aqueous and almost free of volatile species, with only minor amounts of CO_2 and CH_4 rarely detected.

During the whole Jurassic and part of the Cretaceous period, the eastern Paris Basin was immersed (Mégnien et al., 1980). Hence, the presence of seawater within the porosity of the Jurassic limestones during this period is plausible. This hypothesis was invoked by Brigaud et al. (2009a) to account for the $\delta^{18}O$ values of the mesogenetic calcite cements in the Middle Jurassic formations. However, mixing of meteoric water with seawater can only generate a small shift relative to the meteoric water line (*e.g.*, Lynn Ingram et al., 1996), unless one or both compounds is/are strongly enriched during evaporation (Knauth and Beeunas, 1986).

In summary, paleowaters showing a shift to the right of the GMWL can be explained either by an overestimation of the crystallization temperature, which should thus be slightly less than 35 °C, or by an enrichment in ^{18}O through the dissolution of host limestones. The latter process is evidenced at present in the center part of the Paris Basin, where long-term equilibration of groundwater with the Middle Jurassic limestones has led to a mean excess in ^{18}O of about 1.5 ‰ relative to the GMWL (Matray et al., 1994) at temperatures between 55 and 80 °C. The δD values of water trapped in fluid inclusions reveal a clear distinction

between the two studied aquifers (Fig. 6). Oxfordian calcite-forming waters are characterized by δD values ranging from –44.2 to –59.5 ‰, consistent with or slightly higher than the present-day groundwater (Fig. 6). As these waters are of meteoric origin, δD values higher than present-day (–49 to –44 ‰) can be explained by different climatic conditions, and hence different δD values of meteoric waters, at the period of paleowater recharge.

δD values of calcite-forming waters in the Middle Jurassic aquifer are clearly distinct from those obtained from the overlying Oxfordian. The δD values of water trapped in calcite cements of Middle Jurassic samples 569 m and 660 m are close, between –32 and –36 ‰. Such values are consistent with the highest δD values measured in present-day groundwater. Moreover, these waters also display high chlorine concentrations (650 - 2700 $mmol \cdot l^{-1}$) so as they are likely enriched in heavier isotopes by the contribution of evaporated seawater.

Paleowater from Middle Jurassic sample 481 m appears highly enriched in deuterium (δD = –20 ‰). For the water to lie on the GMWL, $\delta^{18}O$ of water has to be calculated at a temperature of 53 °C, which should thus be considered as the minimal temperature for calcite crystallization. This sample also contains saline water trapped as fluid inclusions (Cl concentration between 1000 and 1700 $mmol \cdot l^{-1}$), and may thus correspond to mixing between evaporated seawater and meteoric water.

Evolution of pore water salinity

The chlorinity of paleowater trapped as fluid inclusions in authigenic calcite from the Oxfordian is comparable to present-day groundwaters (Fig. 7). Within the Oxfordian limestones, widespread calcite cementation was induced by tectonically-driven circulation of meteoric waters during Cenozoic times (André et al., 2010). At this period, the eastern part of the Paris Basin was already uplifted and the aquifers subjected to meteoric water recharge. Field observations at the vicinity of the Gondrecourt graben (Augeville and Leurville sites) show that the Oligocene E-W extensional regime favored the precipitation of large amounts of calcite under a highly dynamic fluid flow inferred from the presence of hydrothermal breccias. The salinity of these calcite-forming waters is very low (< 150 $mmol \cdot l^{-1}$), thus showing that brines were absent or highly diluted by fresh waters.

In the Middle Jurassic limestones, by contrast, paleowaters trapped in newly-formed calcite reveal high chlorine content, between 650 and 2700 $mmol \cdot l^{-1}$. Such high salinity is also found in quartz and celestite-hosted fluid inclusions from the Middle and Lower Oxfordian marls and the Bathonian limestones (Table 1). These ranges of values are higher than the average seawater (~ 550 $mmol \cdot l^{-1}$) and thus imply a brine component in the calcite-forming waters. This brine is likely of primary origin (*i.e.*, generated by evaporation of seawater, Hanor, 1994) as no cross-formational flow from the Upper Triassic halite to the Middle or Upper Jurassic aquifer has been evidenced in the eastern Paris Basin (Marty et al., 2003; Battani et al., 2011; Rebeix et al., 2011). Dating of geodic calcite by the U-Pb method has revealed a major precipitation event at 149.2 ± 5.8 Ma, *i.e.*, during the Kimmeridgian/Berriasian period (Pisapia et al., 2011). During the late Jurassic times, the eastern Paris Basin was still immersed and subjected to marine sedimentation. The opening of the central Atlantic Ocean led to the general emersion of the eastern flank of the basin at the end of Jurassic (during the “Late Cimmerian Unconformity”, LCU). The sea regression is marked by a sabkha environment during late Tithonian, with the deposition of evaporites (“Purbeckian” facies, Guillocheau et

al., 2000). In a similar way, an increase of the Jurassic limestones porewater salinity may have occurred during this period.
The present-day chlorine concentration of Middle Jurassic groundwaters is ten to a hundred times lower than those measured in fluid inclusions trapped in calcite cements (Fig. 7). This illustrates the evolution of porewater composition: the brine component has been progressively flushed out and diluted by meteoric water. This gradual change could have started after the definitive retreat of the sea at the end of Cretaceous times.

3. Fluid circulation on a regional scale

δD and $\delta^{18}O$ of calcite-forming water from different outcrops are shown on Fig. 8. The paleowater isotopic domains in the Oxfordian and Middle Jurassic limestone aquifers from the Andra site are also plotted for comparison on the same figure. Samples from Augeville and Leurville (Fig. 8) correspond to hydraulic breccias crosscutting the Upper Oxfordian limestones and formed during the E-W Oligocene extensional stage (André et al., 2010). As illustrated on Fig. 8, the calcite parent-water plots close to the GWML at temperatures around 35 °C. Furthermore, the isotopic composition of this water is comparable to the one of calcite-forming water within the Oxfordian at depth, in the Andra site. Hence, these results strongly suggest a common origin for these calcite infillings, which is also supported by the Eocene-Oligocene age obtained on geodic calcite from Oxfordian cores (U-Pb dating at 33.2 ± 5.5 Ma, Pisapia et al., 2011). It should be noted that the mean temperature range of paleowater from Augeville and Leurville (inferred from the oxygen and hydrogen isotopic composition) is between 31 and 41 °C, while the one from Oxfordian paleowater at depth in the Andra site is slightly lower, between 25 and 36 °C, if one considers a strictly meteoric origin with no ^{18}O enrichment from the dissolution of host rock. Water circulation may have been initiated during the opening of the Gondrecourt Graben along the major faults, with a subsequent lateral percolation through the Oxfordian aquifer and associate cooling. Noteworthy is the fact that the isotopic composition of geodic calcite sampled within the Bajocian limestones from the Sommerécourt quarry is clearly distinct from those of the Middle Jurassic at depth in the Andra site. Instead, the calcite-forming water inferred from Sommerécourt outcrops rather matches the isotopic composition of meteoric water which has cemented the Oxfordian limestones (Fig. 8). The Sommerécourt quarry is located at the vicinity of the Hercynian “Vittel fault”, which was reactivated during the Oligocene extension (André, 2003). Hence, calcite precipitation in these Middle Jurassic limestones likely occurred during the same period as in the Oxfordian limestones (i.e., during Oligocene). Thus, the isotopic composition of the fluid rather marks the process and the period at which large scale water circulation and correlative calcite precipitation occurred, independently of the age of the host rock.

4. Towards a conceptual model of paleowater circulation through time

Two major crystallization events have been characterized in this study:

- During the Late Jurassic/Early Cretaceous period, evidenced by calcite and celestite crystals in the Jurassic limestones, and by chalcedony-quartz-celestite assemblages in the Middle Oxfordian silty-marl layer (*Terrain à Chailles).*
- During the Late Eocene/Oligocene period, evidenced by calcite crystallization in the Upper Oxfordian limestone.

Although not representing the entire paragenetic sequence, these crystallization events are the most significant in terms of cement volumes (Brigaud et al., 2009a; Carpentier et al., 2014) and correspond to two main fluid events. Figure 9 compares the composition of paleowaters with present-day groundwater in a [Cl^-] vs. δD diagram. This underlines that, in the Middle Jurassic aquifer, both dilution and cooling occurred from ~150 Ma to present. As the water residence time was estimated to be in the order of several hundred thousand years, it is more likely that chlorine in present-day groundwater is supplied by the diffusion from underlying Triassic and Lower Jurassic units, rather than inherited from the ~150 Ma brines identified in this study. In the Upper Oxfordian limestone aquifer, Figure 9 illustrates that paleowaters from the Late Eocene/Oligocene period were warmer compared to present-day groundwater. This may be due to advective water flow under high fluid/rock ratios conditions during the Cenozoic rifting events. As a summary, two sketches are proposed in Figures 10 and 11 to illustrate the main crystallization events, the circulation of paleowater related to the successive geodynamic events and the evolution of fluid sources trough time.

Conclusions

In the eastern part of the Paris Basin, the Callovian-Oxfordian claystones are studied for the long-term storage of nuclear wastes (Underground Research Laboratory, ANDRA). Diffusion of gas and solutes from the underlying sedimentary series has erased the original pore water composition. Knowing the evolution of groundwater composition and temperature in the underlying and overlying limestones, from the past geologic times to the present, is a critical step to model the evolution of water advection in limestone aquifers and diffusion through the claystone units. In this study, we have shown that:

- Brines with chlorine concentrations up to 3800 $mmol \cdot l^{-1}$ were involved in calcite cementation within the Middle Jurassic limestones and in calcite-quartz-celestite infillings within the Lower Oxfordian marls. These crystallization events likely occurred during the late Jurassic or early Cretaceous period. By contrast, authigenic calcite crystals in the Oxfordian limestones, crystallized during the Cenozoic times, contain fluid inclusions of lower salinity (< 150 $mmol \cdot l^{-1}$), showing that the brines were flushed out by meteoric water infiltrations during the Cretaceous uplift of the eastern border of the basin.

- The oxygen and hydrogen isotope compositions of paleowater are significantly different between the Oxfordian and the Middle Jurassic limestone aquifers. Regarding the Oxfordian, paleowater dated from the Cenozoic times does not exhibit large difference compared to present-day groundwater. Regarding the Middle Jurassic aquifer, water involved in calcite cementation during the Late Jurassic/Early Cretaceous period was probably warmer (30 – 55 °C) and of mixed meteoric and evaporated marine origin.

- At the regional scale, fluid inclusions from several calcite infillings of Cenozoic age show have δD values close to those determined in the Oxfordian aquifer at depth, reinforcing the hypothesis of a common origin. Water was warmer at the vicinity of major faults and may have cooled down during the lateral percolation through the aquifer.

From a methodological point of view, this study highlights the fact that chemical and isotopic analyses of fluid inclusions in low-temperature authigenic minerals, although challenging, are critical to reconstruct the evolution of groundwater composition and temperature through times.

Acknowledgments

This study is a part of Andra and TAPSS 2000 research program “Present and past transfers in a sedimentary aquifer – aquitard system: a 2000 meters deep drill-hole in the Mesozoic of the Paris Basin”, and was funded by GNR FORPRO. It was supported by an Andra (French Agency for radioactive waste management) PhD grant for the first author. We are grateful to Marie-Camille Caumon (GeoRessources) for assistance on Raman spectroscopy.

References

André, G., 2003. Caractérisation des déformations méso-cénozoïques et des circulations de fluides dans l'Est du Bassin de Paris. PhD Thesis, Université Henri Poincaré, Nancy, 311 pp.

André, G., Hibsch, C., Fourcade, S., Cathelineau, M., Buschaert, S., 2010. Chronology of fracture sealing under a meteoric fluid environment: Microtectonic and isotopic evidence of major Cainozoic events in the eastern Paris Basin (France). Tectonophysics 490, 214–228.

Baker, P.A., Bloomer, S.H., 1988. The origin of celestite in deep-sea carbonate sediments. Geochimica et Cosmochimica Acta 52, 335–339.

Battani, A., Smith, T., Robinet, J.C., Brulhet, J., Lavielle, B., Coelho, D., 2011. Contribution of logging tools to understanding helium porewater data across the Mesozoic sequence of the East of the Paris Basin. Geochimica et Cosmochimica Acta 75, 7566–7584.

Baumgartner, M., Bakker, R.J., 2008. Raman spectroscopy of pure H_2O and NaCl-H_2O containing synthetic fluid inclusions in quartz – a study of polarization effects. Mineralogy and Petrology 95, 1–15.

Bensenouci, F., Michelot, J.L., Matray, J.M., Savoye, S., Tremosa, J., Gaboreau, S., 2013. Profiles of chlorine and stable isotopes in pore-water obtained from a 2000 m-deep borehole through the Mesozoic sedimentary series in the eastern Paris Basin. Physics and Chemistry of the Earth 65, 1–10.

Blaise, T., Izart, A., Michels, R., Suarez-Ruiz, I., Cathelineau, M., Landrein, P., 2011. Vertical and lateral changes in organic matter from the Mesozoic, eastern Paris Basin (France): Variability of sources and burial history. International Journal of Coal Geology 88, 163–178.

Blaise, T., Barbarand, J., Kars, M., Ploquin, F., Aubourg, C., Brigaud, B., Cathelineau, M., El Albani, A., Gautheron, C., Izart, A., Janots, D., Michels, R., Pagel, M., Pozzi, J.P., Boiron, M.C., Landrein, P., 2014. Reconstruction of low temperature (<100 °C) burial in sedimentary basins : A comparison of geothermometer in the intracontinental Paris Basin. Marine and Petroleum Geology 53, 71–87.

Bigeleisen, J., Pearlman, M. L., Preener, H.C., 1952. Conversion of hydrogenic materials to hydrogen for isotopic analysis. Analytical Chemistry 24, 1356–1357.

Bonhomme, M.G., Baubron, J-C., Jebrak, M., 1987. Minéralogie, géochimie, terres rares et âge K-Ar des argiles associées aux minéralisations filoniennes. (Mineralogy, geochemistry, rare earths and K-Ar age of clays associated with vein-type mineralizations). Chemical Geology 65, 321–339.

Brigaud B., Vincent, B., Durlet, C., Deconinck, J.F., Blanc, P., Trouiller, A., 2010. Acoustic properties of ancient shallow-marine carbonates : effects of depositional environments and

diagenetic processes (Middle Jurassic, Paris Basin, France). Journal of Sedimentary Research 80, 791–807.

Brigaud, B., Durlet, C., Deconinck, J-F., Vincent, B., Thierry, J., Trouiller, A., 2009a. The origin and timing of multiphase cementation in carbonates: Impact of regional scale events on the Middle Jurassic Limestones diagenesis (Paris Basin, France). Sedimentary Geology 222, 161–180.

Brigaud, B., Durlet, C., Deconinck, J-F., Vincent, B., Pucéat, E., Thierry, J., Trouiller, A., 2009b. Facies and climate/environmental changes recorded on a carbonate ramp: A sedimentological and geochemical approach on Middle Jurassic carbonates (Paris Basin, France). Sedimentary Geology 222, 181–206.

Boyce, A.J., Fallick, A.E., Hamilton, P.J., Elorza, J., 1990. Diagenesis of celestite in quartz geodes from the Basque-Cantabric Basin, northern Spain: evidence from sulphur and strontium isotopes. Geochemistry of the Earth's surface and of mineral formation 2nd international symposium, July, 2–8, Aix-en-Provence, France.

Buschaert, S., Fourcade, S., Cathelineau, M., Deloule, E., Martineau, F., Ayt Ougougdal, M., Trouiller, A., 2004. Widespread cementation induced by inflow of continental water in the eastern part of the Paris Basin: O and C isotopic study of carbonate cements. Applied Geochemistry 19, 1201–1215.

Buschaert, S., Giannesini, S., Lavastre, V., Benedetti, L., Gaucher, E., Lacroix, M., Lavielle, B., Michelot, J.L., France-Lanord, C., Bourles, D., Lancelot, J., Benabderrahmane, H., Dewonck, S., Vinsot. A., 2007. The contribution of water geochemistry to the understanding of the regional hydrogeological system. Mémoire de la Société Géologique de France 178, 91–114.

Carpentier, C., Lathuilière, B., Ferry, S., 2010. Sequential and climatic framework of the growth and demise of a carbonate platform : implications for the peritidal cycles (Late Jurassic, North-eastern France). Sedimentology 57, 985–1020.

Carpentier, C., Brigaud, B., Blaise, T., Vincent, B., Durlet, C., Boulvais, P., Pagel, M., Hibsch, C., Yven, B., Lach, P., Cathelineau, M., Boiron, M.C., Landrein, P, Buschaert, S., 2014. Impact of basin burial and exhumation on Jurassic carbonates diagenesis on both sides of a thick clay barrier (Paris Basin, NE France). Marine and Petroleum Geology 53, 44–70.

Cathelineau, M., Fourcade, S., Clauer, N., Buschaert, S., Rousset, D., Boiron, M.C., Meunier, A., Lavastre, V., Javoy, M., 2004. Dating multistage paleofluid percolations : A K-Ar and $^{18}O/^{16}O$ study of fracture illites from altered Hercynian plutonites at the basement/cover interface (Poitou High, France). Geochimica et Cosmochimica Acta 68, 2529–2542.

Cathelineau, M., Boiron, M.C., Fourcade, S., Ruffet, Clauer, N., G., Belcourt, O., Coulibaly, Y., Banks, D.A., Guillocheau, F., 2012. A major Late Jurassic fluid event at the basin/basement unconformity in western France: 40Ar/39Ar and K-Ar dating, fluid chemistry, and related geodynamic context. Chemical Geology 322–323, 99–120.

Caumon, M.C., Dubessy, J., Robert, P., Tarantola, A., 2013. Fused-silica capillary capsules (FSCCs) as reference synthetic aqueous fluid inclusions to determine chlorinity by Raman spectroscopy. European Journal of Mineralogy 25, 755–763.

Caumon, M.C., Tarantola, A., Mosser-Rück, R. 2015. Raman spectra of water in fluid inclusions: I. Effect of host mineral birefringence on salinity measurement. Journal of Raman Spectroscopy.

Charef, A., Sheppard, A.M.F., 1987. Pb-Zn mineralization associated with diapirism: fluid inclusion and stable isotope (H,C,O) evidence for the origin and evolution of the fluids at Fedj-el-Adoum, Tunisia. Chemical Geology 61, 113–134.

Chowns, T.M., Elkins, J.E., 1974. The origin of quartz geodes and cauliflower cherts through the silicification of anhydrite nodules. Journal of Sedimentary Petrology 44, 885–903.

Clauer, N., O'Neil, J.R., Furlan, S., 1995. Clay minerals as records of temperature conditions and duration of thermal anomalies in the Paris Basin, France. Clay Minerals 30, 1–13.

Clauer N., Zwingmann H., Chaudhuri S., 1996. Isotope (K-Ar and oxygen) constraints on the extent and importance of the Liassic hydrothermal activity in western Europe. Clay Minerals 31, 301–318.

Clauer, N., Fourcade, S., Cathelineau, M., Girard, J.P., Vincent, B., Elie, M., Buschaert, S., Rousset, D., 2007. A review of studies on the diagenetic evolution of the Dogger to Tithonian sedimentary sequence in the eastern Paris Basin. Impact on the physical and chemical rock properties. Mémoire de la Société Géologique de France 178, 59–71.

Clayton, R.N., Mayeda, T.K., 1963. The use of bromine pentafluoride in the extraction of oxygen from oxides and silicates for isotopic analysis. Geochimica et Cosmochimica Acta 27, 43–52.

Clayton, R.N., Friedman, I., Graf, D.L., Mayeda, T.K., Meents W.F., Shimp, N.F., 1966. The origin of saline formation waters. I. Isotopic composition. Journal of geophysical research 71, 3882–3969.

Craig, H., 1961. Isotopic variations in meteoric waters. Science 133, 1702–1703.

de Haller, A., Tarantola, A., Mazurek, M. and Spangenberg, J., 2011. Fluid flow through the sedimentary cover in northern Switzerland recorded by calcite-celestite veins (Oftringen borehole, Olten). Swiss Journal of Geosciences 104, 493–506.

Demars, C., Pagel., M., 1994. Paleotemperatures and paleosalinities in the Keuper sandstones of the Paris Basin: fluid inclusions in authigenic minerals. Comptes Rendus de l'Académie des Sciences de Paris 319, 427–434.

DeMaster, D.J., 2004. The diagenesis of biogenic silica: Chemical transformations occurring in the water column, seabed, and crust. In: Treatise of Geochemistry, Volume 7 (Ed. F.T. Mackenzie), pp. 87–98.

Dubessy, J., Lhomme, T., Boiron, M.C., Rull, F., 2002. Determination of chlorinity in aqueous fluids using Raman spectroscopy of the stretching band of water at room temperature: application to fluid inclusions. Applied Spectroscopy 56, 99–106.

Dubliansky, Y., 2004. Aspects minéralogiques et géochimiques dans la formation hôte. In. rapport IEER. Examen critique du programme de recherche de l'ANDRA pour déterminer l'aptitude du site de Bure au confinement géologique des déchets à haute activité et à vie longue. Rapport final, 308pp.

Dublyansky, Y.V., Spötl, C., 2009. Hydrogen and oxygen isotopes of water from inclusions in minerals: design of a new crushing system and on-line continuous-flow isotope ratio mass spectrometric analysis. Rapid Communications In Mass Spectroscopy 23, 2605–2613.

Dublyansky, Y.V., Spötl, C., 2010. Evidence for a hypogene paleohydrogeological event at the prospective nuclear waste disposal site Yucca Mountain, Nevada, USA, revealed by the isotope composition of fluid-inclusion water. Earth and Planetary Science Letters 289, 583–594.

Durlet, C., Thierry, J., 2000. Modalités séquentielles de la transgression aalénobajocienne sur le sud-est du Bassin parisien. Bulletin de la Société géologique de France 171, 327–339.

Ferry, S., Pellenard, P., Collin, P.Y., Thierry, J., Marchand, D., Deconinck, J.F., Robin, C., Carpentier, C., Durlet, C., Curial, A., 2007. Synthesis of recent stratigraphic data on Bathonian to Oxfordian deposits of the eastern Paris Basin. Mémoire de la Société Géologique de France 178, 37–57.

Finch, A.A., Allison, N., 2003. Strontium in coral aragonite: 2. Sr coordination and the long-term stability of coral environment records. Geochimica et Cosmochimica Acta 67, 4519–4527.

Folk, R.L., Pittman, J.S., 1971. Length-slow chalcedony: a new testament for vanished evaporites. Journal of Sedimentary Petrology 41, 1045–1058.

Fontes, J.C., Matray, J.M., 1993a. Geochemistry and origin of formation brines from the Paris Basin, France. I. Brines associated with Triassic salts. Chemical Geology 109, 149–175.

Fontes, J.C., Matray, J.M., 1993b. Geochemistry and origin of formation brines from the Paris Basin, France. II. Saline solutions associated with oil fields. Chemical Geology 109, 177–200.

Fourré, E., Jean-Baptiste, P., Dapoigny, A., Lavielle, B., Smith, T., Thomas, B., Vinsot, A., 2011. Dissolved helium distribution in the Oxfordian and Dogger deep aquifers of the Meuse/Haute-Marne area. Physics and Chemistry of the Earth 36, 1511–1520.

Geeslin, J.H., Chafetz, H.S., 1982. Ordovician aleman ribbon cherts: an example of silicification prior to carbonate lithification. Journal of Sedimentary Petrology 52, 1283–1293.

Giannesini, S., 2006. Géochimie isotopique couplée des eaux des formations argileuses et calcaires du site Andra de Meuse/Haute-Marne. PhD thesis. Paul Cezanne Univeristy, Aix-Marseille, France, 291 pp.

Goldstein, R.H., Reynolds, T.J., 1994. Systematics of fluid inclusions in diagenetic minerals. Chapter 6: Fluid inclusion petrography. SEPM Short Course Notes 31, 69–85.

Goldstein, R.H., 2001. Fluid inclusions in sedimentary and diagenetic systems. Lithos 55, 159–193.

Gomez-Alday, J., Garcia-Garmilla, F., Elorza, J., 2002. Origin of quartz geodes from Lano and Tubilla del Algua sections (middle-upper Campanian, Basque-Cantabrian Basin, northern Spain): isotopic differences during diagenetic processes. Geological Journal 37, 117–134.

Gonfiantini, R., 1986. Isotopes in lake studies, in Handbook of Environmental Isotope Geochemistry (P. Fritz and J-Ch. Fontes, Eds.), Vol. 2, pp.113–168.

Guillocheau, F., Robin, C., Allemand, P., Bourquin, S., Brault, N., Dromart, G., Friedenberg, R., Garcia, J.-P., Gaulier, J.- M., Gaumet, F., Grosdoy, B., Hanot, F., Le Strat, P., Mettraux, M., Nalpas, T., Prijac, C., Rigollet, C., Serrano, O., Grandjean, G., 2000. Meso-Cenozoic geodynamic evolution of the Paris Basin: 3D stratigraphic constraints. Geodinamica Acta 13, 189–246.

Hanor, J.S., 1994. Origin of saline fluids in sedimentary basins. In Parnell, J., (ed.), Geofluids: Origin and migration of fluids in sedimentary basins: Geological Society of London Special Publication, 78, 151–174.

Hanor, J.S., 2000. Barite-Célestine geochemistry and environment of formation. In C. Alpers, J. Jambor, and K. Norstrom (Eds), Sulfate minerals. Reviews in Mineralogy and Geochemistry 40, 193–275.

Hanor, J.S., 2004. A model for the origin of large carbonate- and evaporite-hosted celestine ($SrSO_4$) deposits. Journal of Sedimentary Research 74, 168–175.

Hendry, J.P., Trewin, N.H.., 1995. Authigenic quartz microfabrics in Cretaceous turbidites: evidence for silica transformation processes in sandstones. Journal of Sedimentary Research 65, 380–92.

Hendry, M.J., Salomon, D.K., Person, M., Wassenaar, L.I., Gardner, W.P., Clark, I.D., Mayer, K.U., Kunimaru, T., Nakata, N., Hasegawa, T, 2015. Can argillaceous formations isolate nuclear waste? Insights from isotopic, noble gas, and geochemical profiles. Geofluids 15, 381–386.

Hibsch, C., Siebenaller, L., Vennin, E., Cathelineau, M., Techer, I., Fourcade, S., Lavastre, V., Agrinier, P., 2005. Reconstitution des paléo-circulations de fluides et caractérisation des eaux porales actuelles dans le Dogger dans l'environnement du site ANDRA de Meuse/Haute-Marne par analyses isotopiques couplées (C, O, Sr, Cl) et minéralogiques. Minéralogie, Géochimie Isotopique du Sr, du C et de l'O, Géochimie isotopique du Cl. Rapport Final Action de Recherche 2004-1, GdR ForPro, 82 pp.

Hoareau, G., Monnin, C., Odonne, F., 2010. A study of celestine equilibrium in marine sediments using the entire ODP/IODP porewater data base. Geochimica et Cosmochimica Acta 74, 3925–3937.

IAEA, 2000a. Environmental Isotopes in the Hydrological Cycle. Principles and Applications Ed. Mook, W.G., Volume 2: Atmospheric Water.

IAEA, 2000b. Environmental Isotopes in the Hydrological Cycle. Principles and Applications Ed. Mook, W.G., Volume 4: Groundwater.

Jones, C.E., Jenkyns, H.C., Hesselbo, S.P., 1994. Strontium isotopes in Early Jurassic seawater. Geochimica et Cosmochimica Acta 58, 1285–1301.

Jones, C.E., Jenkyns, H.C., Coe, A.L., Hesselbo, S.P., 1994. Strontium isotopic variations in Jurassic and Cretaceous seawater. Geochimica et Cosmochimica Acta 58, 3061–3074.

Kharaka, Y.K., Carothers, W.W., 1986. Oxygen and hydrogen isotope geochemistry of deep basin brines. In *Handbook of Environmental Isotope Geochemistry*, eds J. C. Fritz and P. Fontes, volume 2, pp. 305–360. Elsevier, Amsterdam.

Kharaka, Y.K., Thordsen, J.J., 1992. Stable isotpe geochemistry and origin of waters in sedimentary basins, in Clauer, N. and Chaudouri, S., eds., Isotope signatures and sedimentary records: Germany, Springer-Verlag, pp. 441–466.

Kita, I., Taguchi, S., Matsubaya, O., 1985. Oxygen isotope fractionation between amorphous silica and water at 34 – 93 °C. Nature 314, 83–84.

Knauth, L.P., Beeunas, M.A., 1986. Isotope geochemistry of fluid inclusions in Permian halite with implications for the isotopic history of ocean water and the origin of saline formation waters. Geochimica et Cosmochimica Acta 50, 419–433.

Krüger, Y., Marti, D., Hidalgo Staub, R., Fleitmann, D., Frenz, M., 2011. Liquid–vapour homogenisation of fluid inclusions in stalagmites: Evaluation of a new thermometer for palaeoclimate research. Chemical Geology 289, 39–47.

Lancelot, J.R., De Saint André, B., De la Boisse, H., 1984. Systématique U-Pb et évolution du gisement d'Uranium de Lodève (France). Mineralium Deposita 19, 44–53.

Landrein, P., Vigneron, G., Delay, J., Lebon, P., Pagel M., 2013. Lithology, hydrodynamism and thermicity in the multi-layer sedimentary system intersected by the Andra deep borehole of Montiers-sur-Saulx (Meuse, France). Bulletin de la Société Géologique de France 184, 519–543.

Lavastre, V., Jendrzejewski, N., Agrinier, P., Javoy, M., Evrard, M., 2005. Chlorine transfer out of a very low permeability clay sequence (Paris Basin, France): ^{35}Cl and ^{37}Cl evidence. Geochimica et Cosmochimica Acta 69, 4949–4961.

Lavastre, V., Le Gal La Salle, C., Michelot, J.L., Giannesini, S., Benedetti, L., Lancelot, J., Lavielle, B., Massault, M., Thomas, B., Gilabert, E., Bourlès, D., Clauer, N., Agrinier, P., 2010. Establishing constraints on groundwater ages with ^{36}Cl, ^{14}C, ^{3}H, and noble gases: A case study in the eastern Paris basin, France. Applied Geochemistry 25, 123–142.

Lavastre, V., Ader, M., Buschaert, S., Petit, E., Javoy, M., 2011. Water circulation control on carbonate-$\delta^{18}O$ records in a low permeability clay formation and surrounding limestones: The Upper Dogger–Oxfordian sequence from the eastern Paris basin, France. Applied Geochemistry 26, 818–827.

Lefort, A., Lathuilière, B., Carpentier, C., Huault, V., 2011. Microfossil assemblages and relative sea-level fluctuations in a lagoon at the Oxfordian/Kimmeridgian boundary (Upper Jurassic) in the eastern part of the Paris Basin. Facies 57, 649–662.

Lerouge, C., Grangeon S., Gaucher, E.C., Tournassat, C., Agrinier P., Guerrot, C., Widory D., Fléhoc, C., Wille, G., Ramboz, C., Vinsot, A., Buschaert, S., 2011. Mineralogical and isotopic record of biotic and abiotic diagenesis of the Callovian-Oxfordian clayey formation of Bure (France). Geochimica et Cosmochimica Acta 75, 2633–2963.

Linard, Y., Vinsot, A., Vincent, B., Delay, J., Wechner, S., De La Vaissière, R., Scholz, E., Garry, B., Lundy, M., Cruchaudet, M., Dewonck, S., Vigneron, G., 2011. Water flow in the Oxfordian and Dogger limestone around the Meuse/Haute-Marne Underground Research Laboratory. Physics and Chemistry of the Earth 36, 1450–1468.

Lynn Ingram, B., Conrad, M.E., Ingle, J.C., 1996. Stable isotope and salinity systematics in estuarine waters and carbonates: San Francisco Bay. Geochimica et Cosmochimica Acta 60, 455–467.

Maes, P., 2002. Circulations de fluides et interactions eau/roche passées et actuelles dans la pile sédimentaire du site de Meuse/Haute-Marne: apport des isotopes du Sr et conséquences. PhD Thesis, Université Montpellier, Montpellier, 308 pp.

Madsen, H.B., Stemmerik, L., Surlyk, F., 2010. Diagenesis of silica-rich mound-bedded chalk, the Coniacian Arnager Limestone, Denmark. Sedimentary Geology 223, 51–60.

Marty, B., Dewonck, S., France-Lanord, C., 2003. Geochemical evidence for efficient aquifer isolation over geological timeframes. Nature 425, 55–58.

Matray, J.M., Fontes, J.C., 1990. Origin of the oil-field brines in the Paris Basin. Geology 18, 501–504.

Matray, J.M., Lambert, M., Fontes, J.C., 1994. Stable isotope conservation and origin of saline waters from the Middle Jurassic aquifer of the Paris Basin, France. Applied Geochemistry 9, 297–309.

Mazurek, M., 1999. Evolution of gas and aqueous fluid in low-permeability argillaceous rocks during uplift and exhumation of the central Swiss Alps. Applied Geochemistry 15, 211–234.

Mazurek, M., Alt-Epping, P., Bath, A., Gimmi, T., Waber, N., Buschaert, S., De Cannière, P., De Craen, M., Gautschi, A., Savoye, S., Vinsot, A., Wemaere, I., Wouters, L., 2011. Natural tracer profiles across argillaceous formations. Applied Geochemistry 26, 1035–1064.

McGarry, S., Bar-Matthews, M., Matthews, A., Vaks, A., Schilman, B., Ayalon, A., 2004. Constraints on hydrological and paleotemperatures variations in the Eastern Mediterranean region in the last 140 ka given by the δD values of speleothem fluid inclusions. Quaternary Science Reviews 23, 919 – 934.

Mégnien, C., Mégnien, F., Debrand-Passard, S., 1980. Synthèse Géologique du Bassin de Paris. Mémoires du B.R.G.M., 101, 102, 103, Orléans, 460 pp.

Milliken, K.L., 1979. The silicified evaporite syndrome – two aspects of silicification history of former evaporite nodules from southern Kentucky and northern Tennessee. Journal of Sedimentary Petrology 49, 245–256.

Millot, R., Guerrot, C., Innocent, C., Négrel, P., Sanjuan, B., 2011. Chemical, multi-isotopic (Li-B-Sr-U-H-O) and thermal characterization of Triassic formation waters from the Paris Basin. Chemical Geology 283, 226–241.

Munoz, M., Boyce, A.J., Courjault-Rade, P., Fallick, A.E., Tollon, F., 1999. Continental basinal origin of ore fluids from southwestern Massif central fluorite veins (Albigeois, France): evidence from fluid inclusion and stable isotope analyses. Applied Geochemistry 14, 447–458.

Pin, C., Joannon, S., Bosq, C., Le Fèvre, B., Gauthier, P-J., 2003. Precise determination of Rb, Sr, Ba, and Pb in geological materials by Isotope Dilution and ICP-Quadrupole Mass Spectrometry following selective separation of the analytes. Journal of Analytical Atomic Spectrometry 18, 135–141.

Pinti, D.L., Marty, B., Andrews, J.N., 1997. Atmosphere-derived nobe gas evidence for the preservation of ancient waters in sedimentary basins. Geology 25, 111–114.

Pisapia, C., Deschamps, P., Hamelin, B., Battani, A., Buschaert, S., David, J., 2011. U/Pb dating of geodic calcites: A tool for paleohydrological reconstructions. Goldschmidt abstract, international conference.

Quesnel, F., 2003. Paleoweathering and paleosurfaces from northern and eastern France to Belgium and Luxembourg. Géologie de la France 1, 95–104.

Rebeix, R., Le Gal La Salle, C., Michelot, J.L., Verdoux, P., Noret, A., Monvoisin, G., Gianesinni, S., Lancelot, J., Simler, R., 2011. Tracing the origin of water and solute transfers in deep groundwater from Oxfordian, Dogger and Trias formations in the east of the Paris Basin – France. Physics and chemistry of the Earth 36, 1496–1510.

Respaut, J.P., Cathelineau, M., Lancelot, J.R., 1991. Multistage evolution of the Pierres plantées uranium ore deposit (Margeride, France): Evidence from mineralogy and U-Pb systematic. European Journal of Mineralogy 3, 85–103.

Rousset, D., Clauer, N., 2003. Discrete clay diagenesis in a very low-permeable sequence constrained by an isotopic (K-Ar and Rb-Sr) study. Contribution to Mineralogy and Petrology 145, 182–198.

Sandström, B., Tullborg, E.L., 2009. Episodic fluid migration in the Fennoscandian Shield recorded by stable isotopes, rare earth elements and fluid inclusions in fracture minerals at Forsmark, Sweden. Chemical Geology 266, 126–142.

Shepherd, T.J., Naden, J., Chenery, S.R., Milodowski, A.E., Gillespie, M.R., 2000. Chemical analysis of paleogroundwaters: a new frontier for fluid inclusion research. Journal of Geochemical Exploration 69-70, 415–418.

Sheppard, S.M.F., 1986. Characterization and Isotopic Variations in Natural Waters. Reviews in Mineralogy and Geochemistry 16, 165–183.

Schoell, M, 1980. The hydrogen and carbon isotopic composition of methane from natural gases of various origins. Geochimica et Cosmochimica Acta 44, 649–661.

Tarantola, A., Mullis, J., Vennemann, T., Dubessy, J., de Capitani, C., 2007. Oxidation of methane at the CH_4/H_2O – (CO_2) transition zone in the external part of the Central Alps, Switzerland: Evidence from stable isotope investigations. Chemical Geology 237, 329–357.

Tarantola, A., Caumon, M.C., 2015. Raman spectra of water in fluid inclusions: II. Effect of negative pressure on salinity measurement. Journal of Raman Spectroscopy. DOI 10.1002/jrs.4668

Ulmer-Scholle, D.S., Scholle, P.A., Brady, P.V., 1993. Silicification of evaporites in Permian (Guadalupian) back-reef carbonates of the Delaware Basin, West Texas and New Mexico. Journal of Sedimentary Petrology 63, 955–965.

Vincent, B., Emmanuel, L., Houel, P., Loreau, J.-P., 2007. Geodynamic control on carbonate diagenesis: Petrographic and isotopic investigation of the Upper Jurassic formations of the Paris Basin (France). Sedimentary Geology 197, 267–289.

Williams, L.A., Parks, G.A., Crerar, D.A., 1985. Silica diagenesis, I. solubility controls. Journal of Sedimentary Petrology 55, 301–311.

Wong, W.W., Cabreara, M.P., Klein, P.D., 1984. Evaluation of a dual mass spectrometer system for rapid simultaneous determination of hydrogen-2/hydrogen-1 and oxygen-18/oxygen-16 ratios in aqueous samples. Analytical Chemistry 56, 1852–1858.

Worden, R.H., Matray, J.-M., 1995. Cross formational flow in the Paris Basin. Basin Research 7, 53–66.

Worden, R.H., Coleman, M.L., Matray, J.M., 1999. Basin scale evolution of formation waters: a diagenetic and formation water study of the Triassic Chaunoy Formation, Paris Basin. Geochimica and Cosmochimica Acta 63, 2513–2528.

Zhang, R., Schwarcz, H.P., Ford, D.C., Schroeder, F.S., Beddows, P.A., 2008. An absolute paleotemperature record from 10 to 6 Ka inferred from fluid inclusion D/H ratios of a stalagmite from Vancouver Island, British Columbia, Canda. Geochimica et Cosmochimica Acta 72, 1014–1026.

Zheng, Y.F., 1993. Calculation of oxygen isotope fractionation in anhydrous silicate minerals. Geochimica et Cosmochimica Acta 57, 1079–1091.

Zheng, Y.F., 1999. Oxygen isotope fractionation in carbonate and sulfate minerals. Geochemical Journal 33, 109–126.

Ziegler, P.A., 1990. Geological Atlas of Western and Central Europe. Shell International Petroleum Meeting, The Hague. Distributed by Geological Society Publication House, Bath, 239 pp.

Figure caption

Figure 1. Simplified geological map of the Paris Basin with detailed views of the study area and location of the studied boreholes and outcrops. A. The Paris Basin and its border Hercynian massifs. B. Geological map of the eastern edge of the Paris Basin with major structural features and location of the studied outcrops (star symbols). C. Andra Underground Research Laboratory (URL), with the location of all studied boreholes (EST, PPA, PAX and HTM). D. Simplified lithostratigraphic column of the Jurassic sedimentary sequence, with the position of all studied samples. White squares symbolize quartz-celestite assemblages, grey circles calcite samples.

Figure 2. Burial history diagram with color-scale temperatures (modified from Blaise et al., 2014). Red lines delimit the sequence of interest for the present study.

Figure 3. Petrographic observations.
A. Hand specimen of a compaction crack filled by quartz and celestite (PAX – 324 m, Middle Oxfordian). B. Vug filled by calcite spars (HTM102 – 141 m). C. Paragenetic sequence: Calcite spar fringes ("Spar 1"), chalcedony, micro-quartz and celestite (sample PAX – 324 m, Middle Oxfordian). D. Same as A., SEM – backscattered electron image. E. Cathodoluminescence observation revealing pseudomorphs of lamellar crystals, likely gypsum or anhydrite (EST205 borehole sample, Lower Oxfordian). F. Paragenetic sequence showing chalcedony crosscutting calcite fringes and euhedral quartz crystals. Calcite is stained with an alizarin solution, and the color gradation from purple (core) to blue (edge) shows the increase of the Fe/Mg ratio during crystallization (EST205 borehole sample, Lower Oxfordian). G. SEM – secondary electron picture showing euhedral calcite spar on euhedral quartz (sample PAX – 380 m, Middle Oxfordian). H. Cross-polarized light microphotograph showing a fissure filled with calcite ("spar 2") crosscutting both celestite and chalcedony (sample EST413 – 376 m, Middle Oxfordian).

Figure 4. A. Fluid inclusion planes distributed along concentric growth zone, witnessing their primary origin (calcite sample AB7). B. Typical small-sized primary aqueous liquid inclusions in calcite exhibiting a single phase at room temperature (sample PPA – 134 m, Upper Oxfordian). C. Fluid inclusion planes (FIP) parallel or aligned at 120° relative to the cleavage planes of calcite (sample PPA – 134 m, Upper Oxfordian). Note that the fluid inclusion planes do not crosscut the crystal border, indicating a primary origin (circle). D. One-phase aqueous inclusions in a celestite crystal (sample PAX – 324 m, Middle Oxfordian).

Figure 5. $\delta^{18}O$ values of parent-waters for the paragenetic sequence of sample PAX – 324 m (Middle Oxfordian), calculated from $\delta^{18}O$ of each mineral, using the equations of fractionation of Zheng (1999) for calcite in bulk claystone and late calcite spar, Kita et al. (1985) for chalcedony, and Zheng (1993) for quartz. Calculations were made assuming crystallization temperatures of 35 ± 5 °C (error bars).

Figure 6. Plot of δD vs. $\delta^{18}O$ (‰ $_{V\text{-}SMOW}$) of calcite-parent waters from Oxfordian and Middle Jurassic core samples. $\delta^{18}O$ values of water are calculated from $\delta^{18}O$ of calcite, considering crystallization temperatures at 35 °C (Zheng, 1999). The temperatures of crystallization necessary for the calculated water to lie on the GMWL are indicated. Light blue and deep

blue ellipses symbolized the isotopic domain of present-day groundwater in the Oxfordian and Middle Jurassic aquifers, respectively (Rebeix et al., 2011). GMWL: Global Meteoric Water Line (Craig, 1961); SMOW: Standard Mean Ocean Water.

Figure 7. Ranges of chlorinity values ($mmol \cdot l^{-1}$) of present-day groundwater and paleowater trapped as fluid inclusions in the aquifers of the Paris Basin. Seawater (SW) and halite saturation values after Fontes and Matray (1993a). When indicated, the error bars illustrate minimal and maximal values measured on fluid inclusions by a given study, where the thick part represents the statistically more representative values. Numbers in parentheses indicate references as follows: (1) Rebeix et al. 2011; (2) Matray et al., 1994; (3) Worden and Matray, 1995; (4) Millot et al., 2011; (5) Fontes and Matray, 1993b; (6) Demars and Pagel, 1994. FI: Fluid inclusions; PB: Paris basin. Light green color is used for the data of this study; deep green color shows present-day groundwater in the study area; orange color represents data from the central part of the Paris Basin.

Figure 8. Plot of δD vs. $\delta^{18}O$ (‰ $_{V\text{-}SMOW}$) of calcite-parent water from vug and fracture samples within outcropping Oxfordian and Middle Jurassic limestones. $\delta^{18}O$ values of water are calculated from $\delta^{18}O$ of calcite, considering crystallization temperatures at 35 °C (Zheng, 1999). The temperatures of crystallization to plot the water along the GMWL are indicated. Light blue and deep blue ellipses symbolized the isotopic domain of present-day groundwater in the Oxfordian and Middle Jurassic aquifers, respectively (Rebeix et al., 2011). Light blue and deep blue parallelograms symbolize the isotopic domain of paleowater determined from core samples of Oxfordian and Middle Jurassic limestones, respectively. A maximum deviation of 1.5 ‰ from the equilibration of water with host limestones is assumed. GMWL: Global Meteoric Water Line (Craig, 1961).

Figure 9. Plot of [Cl-] ($mmol.l^{-1}$) vs. δD (‰ $_{V\text{-}SMOW}$) measured in fluid inclusions trapped in authigenic calcite and celestite, defining the domain of composition of paleowaters. Arrows show the evolution of porewater composition from the crystallization period to the present.

Figure 10. Conceptual model showing the origin of brines identified in fluid inclusions trapped in authigenic quartz, celestite and calcite crystals in the Oxfordian and Middle Jurrasic limestones. The upper part of the figure shows a cross-section of the Paris Basin (not to scale), and major geodynamical events during the Kimmeridgian-Berriasian period.

Figure 11. Conceptual model showing the origin of waters identified in fluid inclusions trapped in authigenic calcite crystals during the Oligocene. The upper part of the figure shows a cross-section of the Paris Basin (not to scale), and major geodynamical events. At that time, the sedimentary series were already dipping

Table caption

Table 1. Oxygen and carbon isotope composition of minerals and fluid inclusion isotopic data and chlorinity in authigenic crystals from core (upper part of the table) and outcrop samples (lower part). For some samples, the $\delta^{18}O$ value of calcite has been measured on one fraction and the obtained value was applied to the other fractions (in which case “id.” is indicated). The D/H ratio of sample labeled “481 m” was measured twice: in this specific case, the second sample “481 m -2” is a duplicated measurement (“dupl.”). Symbol “/” indicates all other missing values (analyses not performed). $\delta^{18}O_{H2O}$ values correspond to $\delta^{18}O$ of parent-waters considering crystallization temperatures of 35 °C using the fractionation equation for calcite-H_2O of Zheng (1999). The range of chlorinity values is indicated with the number of analyses within parentheses.

Table 2. Oxygen, carbon and strontium isotope compositions of authigenic minerals measured on core samples. $\delta^{18}O_{H2O}$ values correspond to $\delta^{18}O$ of parent-waters considering crystallization temperatures of 35 °C using the fractionation equation for calcite-H_2O of Zheng (1999). These samples were in too small quantities for the chlorinity and isotopic study of fluid inclusions.

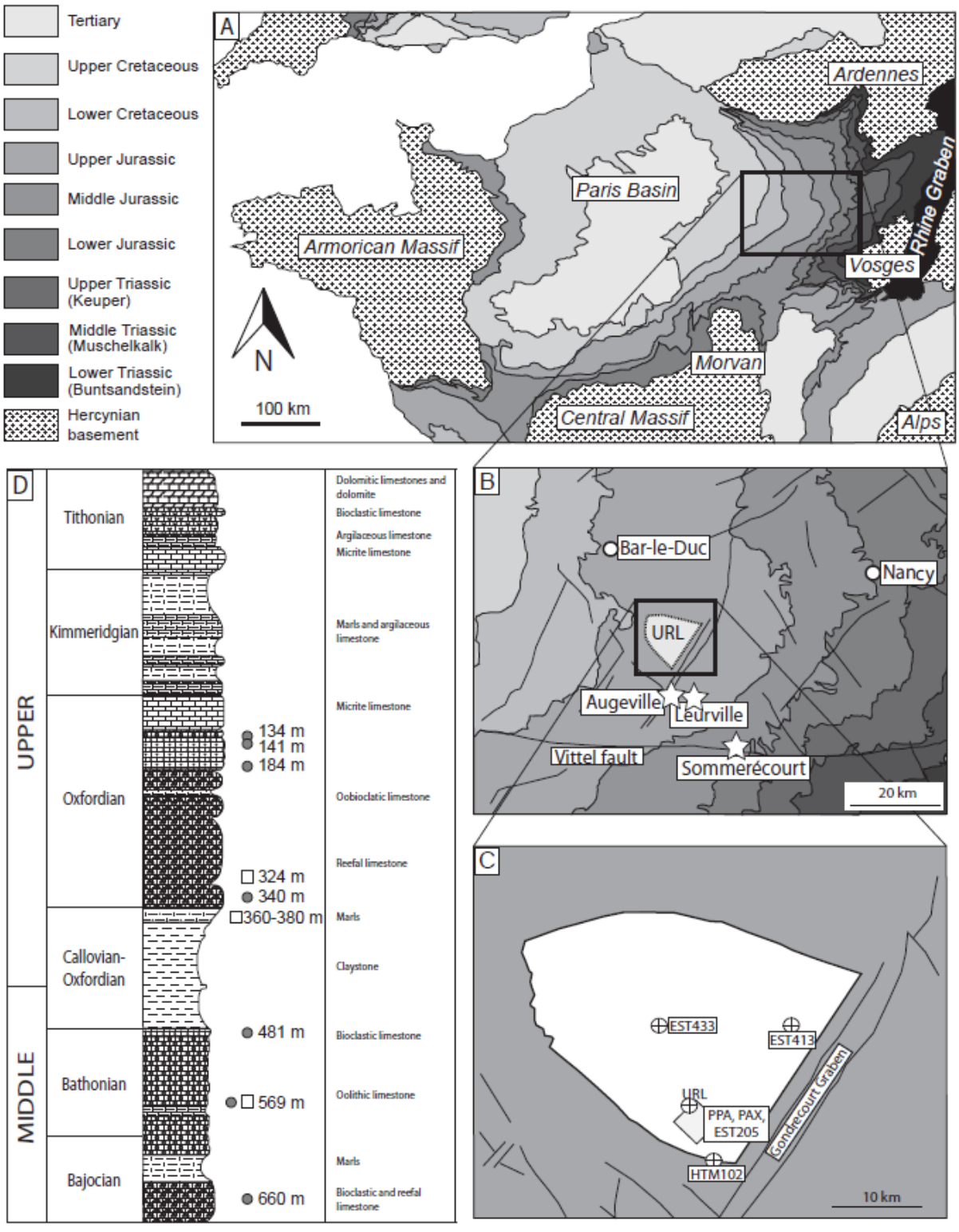
Tertiary
Upper Cretaceous
Lower Cretaceous
Upper Jurassic
Middle Jurassic
Lower Jurassic
Upper Triassic (Keuper)
Middle Triassic (Muschelkalk)
Lower Triassic (Buntsandstein)
Hercynian basement
A
Ardennes
Paris Basin
Rhine Graben
Armorican Massif
Vosges
N
Morvan
100 km
Central Massif
Alps
B
Bar-le-Duc
Nancy
URL
Augeville
Leurville
Vittel fault
Sommerécourt
20 km
C
EST433
EST413
URL
PPA, PAX, EST205
Soncourt graben
HTM102
10 km
D
UPPER
MIDDLE
Tithonian
Kimmeridgian
Oxfordian
Callovian-Oxfordian
Bathonian
Bajocian
134 m
141 m
184 m
324 m
340 m
360-380 m
481 m
569 m
660 m
Dolomitic limestones and dolomite
Bioclastic limestone
Argillaceous limestone
Micrite limestone
Marls and argillaceous limestone
Micrite limestone
Oobioclatic limestone
Reefal limestone
Marls
Claystone
Bioclastic limestone
Oolithic limestone
Marls
Bioclastic and reefal limestone

Fig. 1

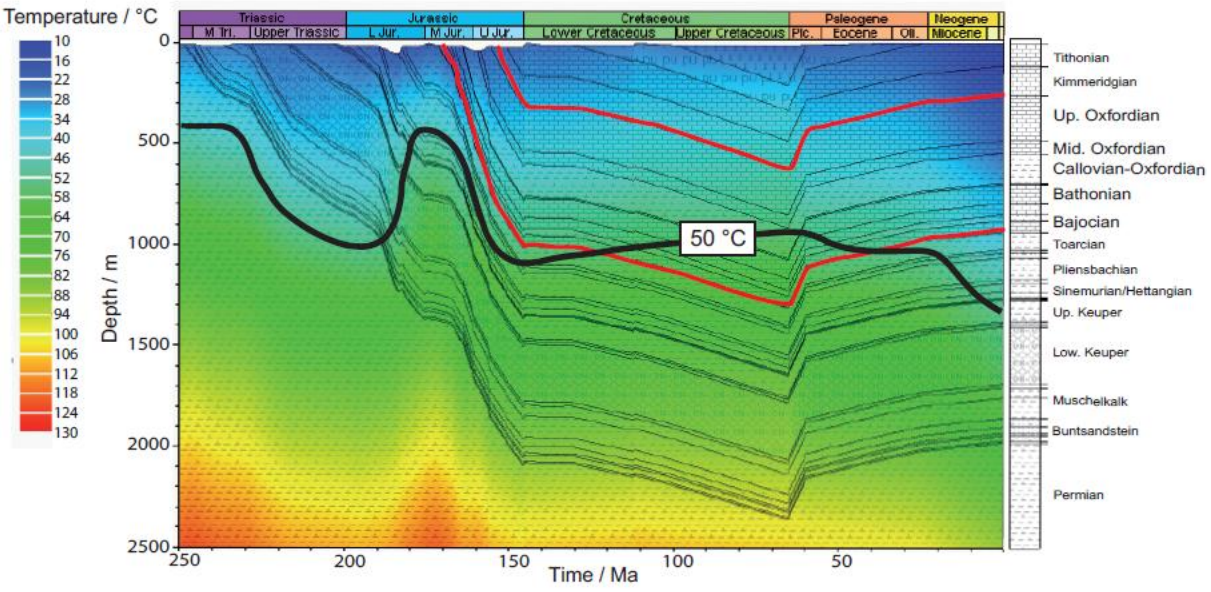
Temperature / °C
10
16
22
28
34
40
46
52
58
64
70
76
82
88
94
100
106
112
118
124
130
Triassic
M Tri.
Upper Triassic
Jurassic
L Jur.
M Jur.
U Jur.
Cretaceous
Lower Cretaceous
Upper Cretaceous
Paleogene
Plc.
Eocene
Oli.
Neogene
Miocene
Depth / m
0
500
1000
1500
2000
2500
50 °C
250
200
150
100
50
Time / Ma
Tithonian
Kimmeridgian
Up. Oxfordian
Mid. Oxfordian
Callovian-Oxfordian
Bathonian
Bajocian
Toarcian
Pliensbachian
Sinemurian/Hettangian
Up. Keuper
Low. Keuper
Muschelkalk
Buntsandstein
Permian

Fig. 2

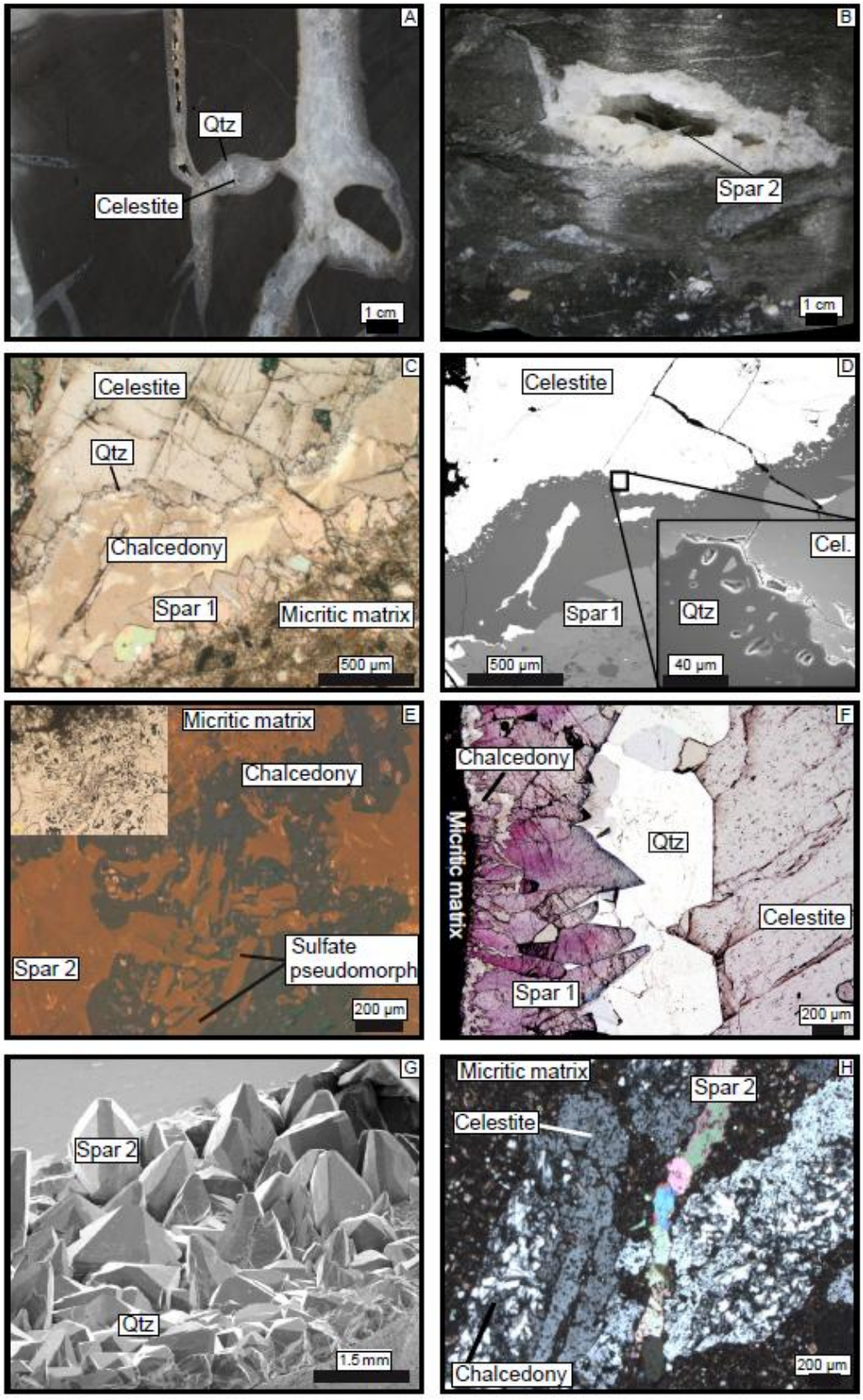
A
Qtz
Celestite
1 cm
B
Spar 2
1 cm
C
Celestite
Qtz
Chalcedony
Spar 1
Micritic matrix
500 µm
D
Celestite
Cel.
Spar 1
Qtz
500 µm
40 µm
E
Micritic matrix
Chalcedony
Spar 2
Sulfate pseudomorph
200 µm
F
Chalcedony
Micritic matrix
Qtz
Celestite
Spar 1
200 µm
G
Spar 2
Qtz
1.5 mm
H
Micritic matrix
Spar 2
Celestite
Chalcedony
200 µm

Fig. 3

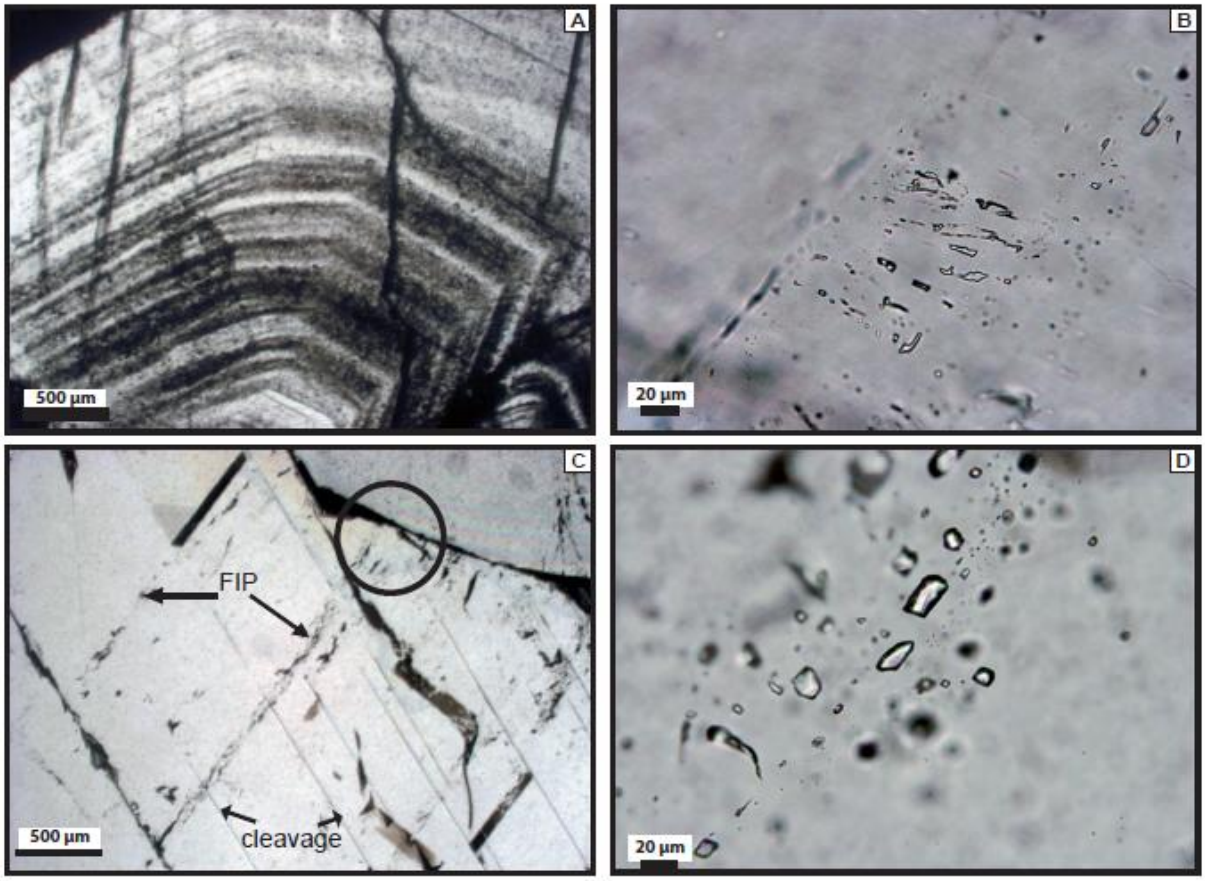

Fig. 4

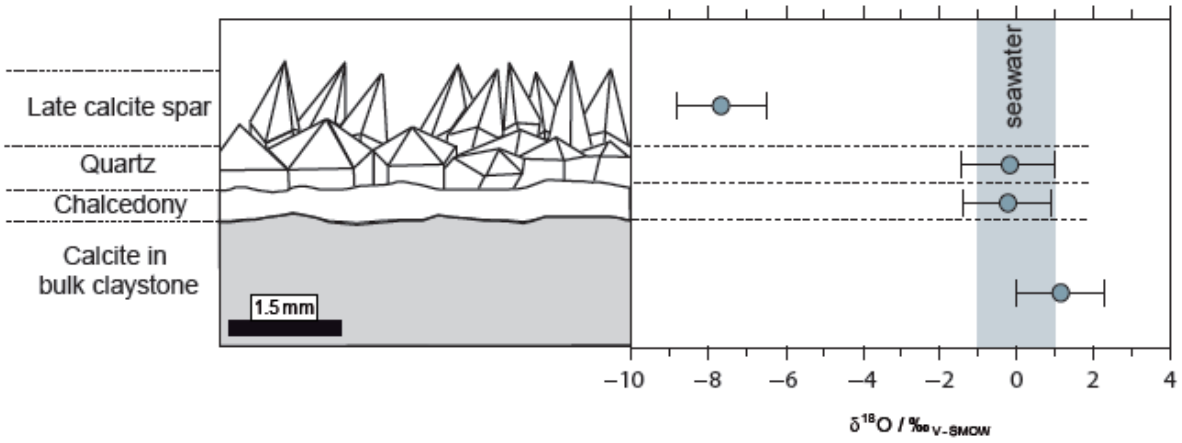
Late calcite spar
Quartz
Chalcedony
Calcite in
bulk claystone
1.5 mm
seawater
−10
−8
−6
−4
−2
0
2
4
δ18O / ‰V-SMOW

Fig. 5

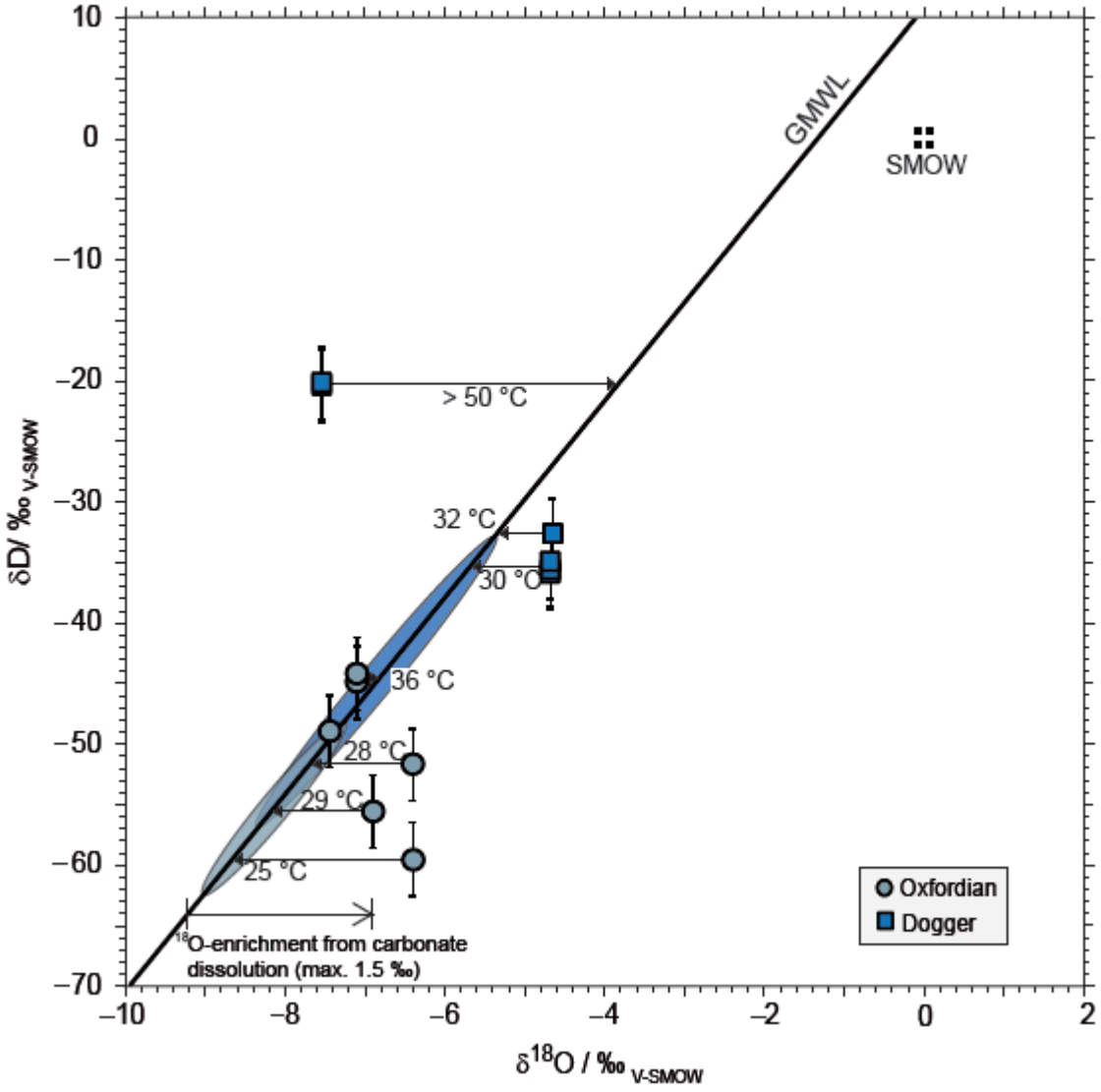
GMWL
SMOW
> 50 °C
32 °C
30 °C
36 °C
28 °C
29 °C
25 °C
18O-enrichment from carbonate dissolution (max. 1.5 ‰)
Oxfordian
Dogger
δD/ ‰ V-SMOW
δ18O / ‰ V-SMOW
10
0
−10
−20
−30
−40
−50
−60
−70
−10
−8
−6
−4
−2
0
2

Fig. 6

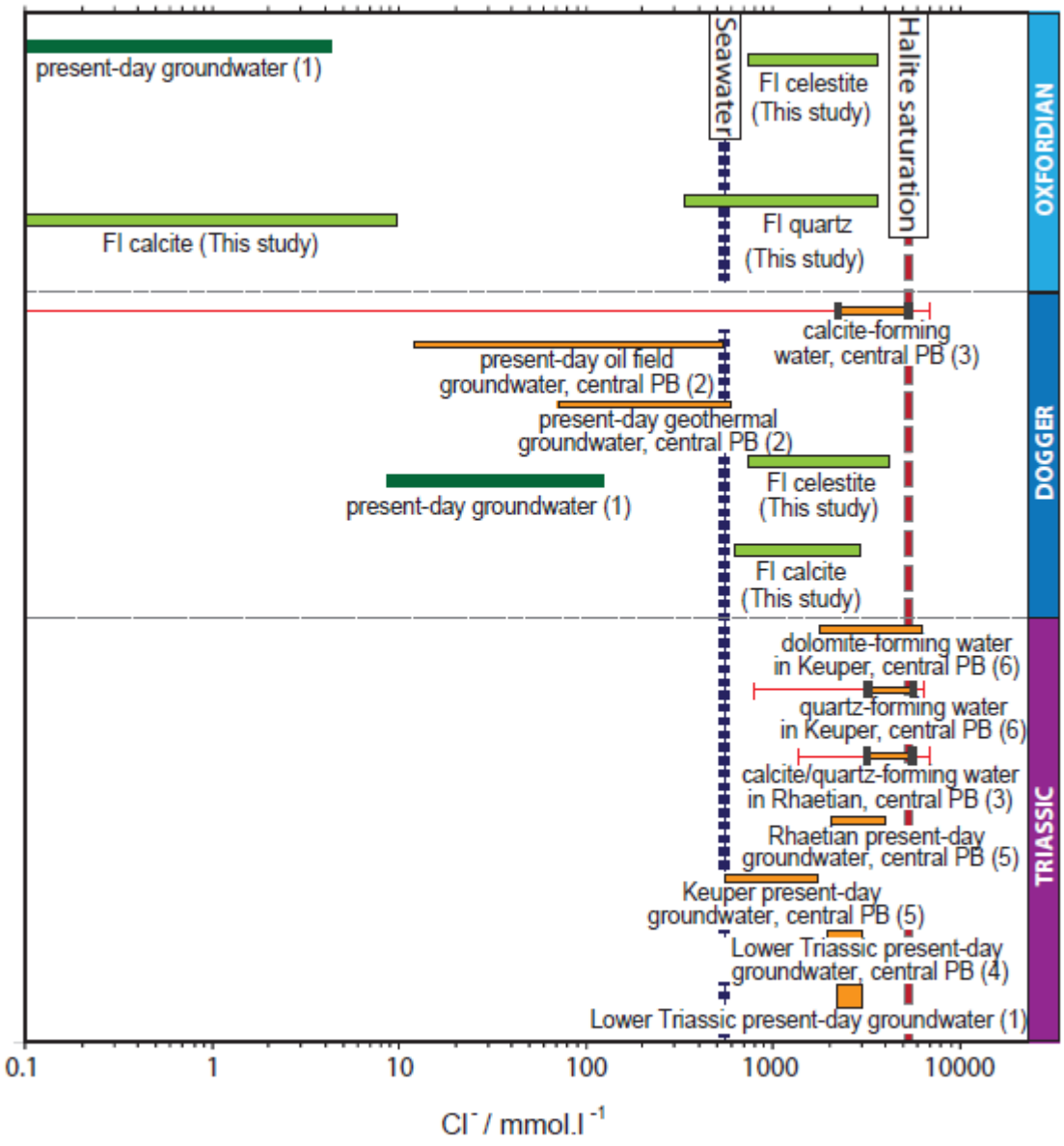
present-day groundwater (1)
Fl calcite (This study)
Seawater
Fl celestite
(This study)
Halite saturation
Fl quartz
(This study)
OXFORDIAN
calcite-forming
water, central PB (3)
present-day oil field
groundwater, central PB (2)
present-day geothermal
groundwater, central PB (2)
present-day groundwater (1)
Fl celestite
(This study)
Fl calcite
(This study)
DOGGER
dolomite-forming water
in Keuper, central PB (6)
quartz-forming water
in Keuper, central PB (6)
calcite/quartz-forming water
in Rhaetian, central PB (3)
Rhaetian present-day
groundwater, central PB (5)
Keuper present-day
groundwater, central PB (5)
Lower Triassic present-day
groundwater, central PB (4)
Lower Triassic present-day groundwater (1)
TRIASSIC
0.1
1
10
100
1000
10000
Cl⁻ / mmol.l⁻¹

Fig. 7

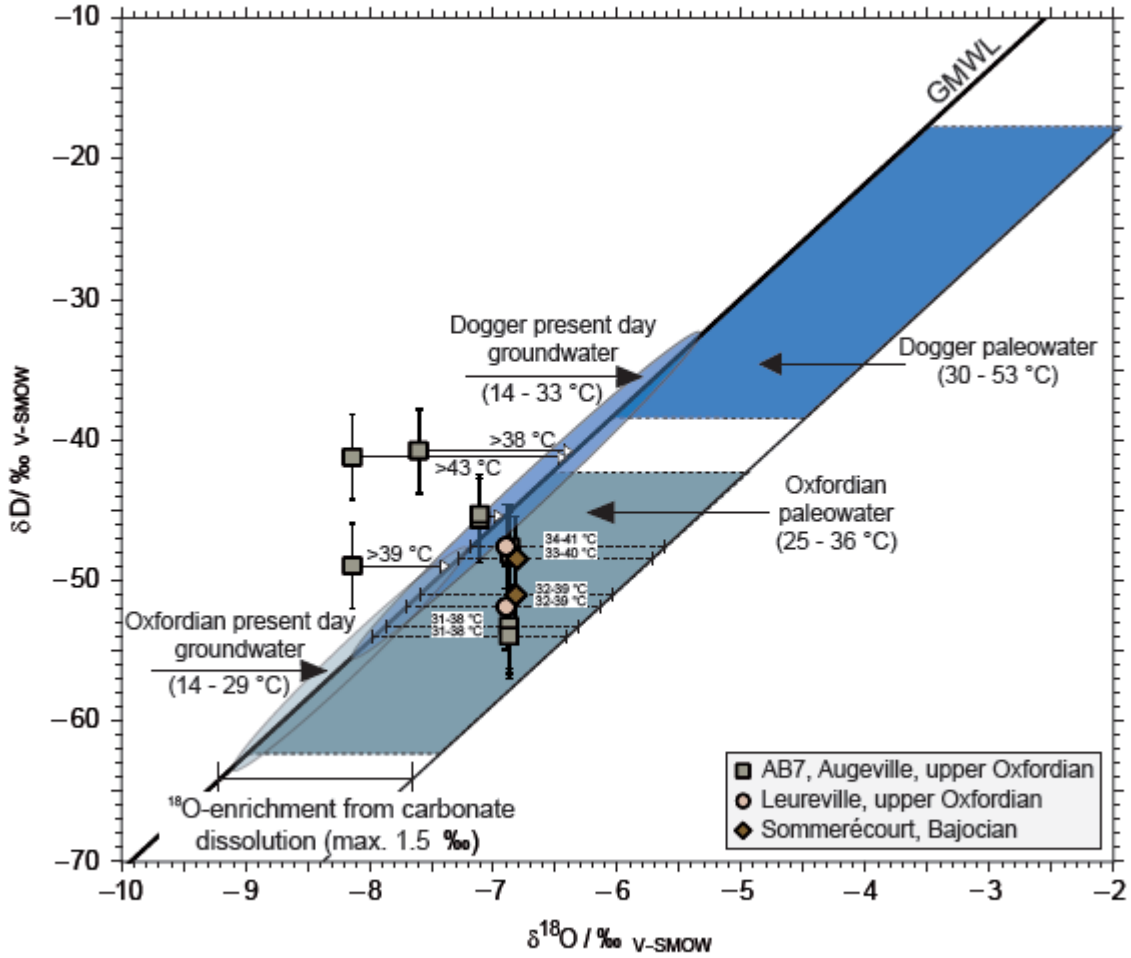
GMWL
Dogger present day groundwater
(14 - 33 °C)
Dogger paleowater
(30 - 53 °C)
>38 °C
>43 °C
Oxfordian paleowater
(25 - 36 °C)
>39 °C
34-41 °C
33-40 °C
32-39 °C
32-39 °C
31-38 °C
31-38 °C
Oxfordian present day groundwater
(14 - 29 °C)
18O-enrichment from carbonate dissolution (max. 1.5 ‰)
AB7, Augeville, upper Oxfordian
Leureville, upper Oxfordian
Sommerécourt, Bajocian
δD/ ‰ V-SMOW
δ18O / ‰ V-SMOW
−10
−20
−30
−40
−50
−60
−70
−10
−9
−8
−7
−6
−5
−4
−3
−2

Fig. 8

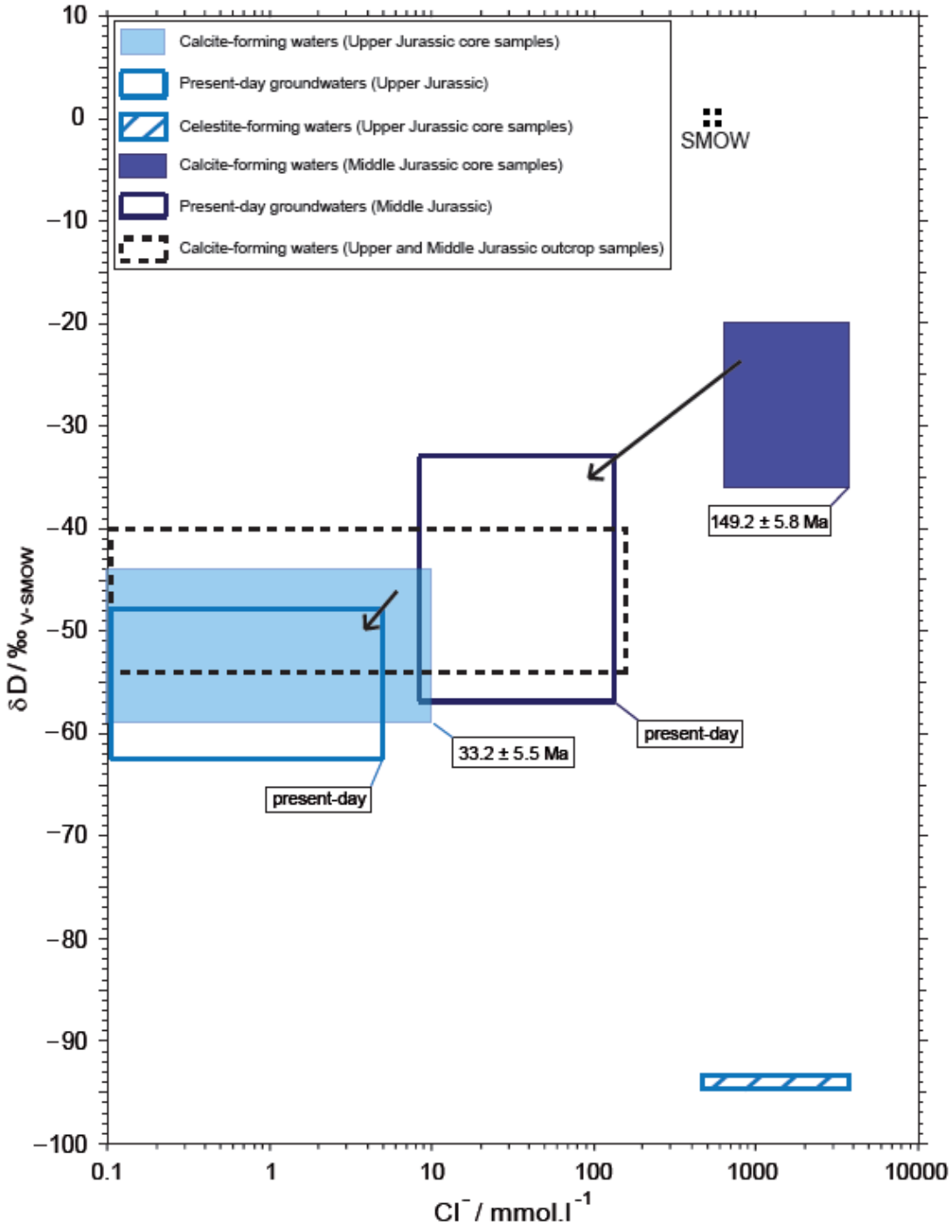
Calcite-forming waters (Upper Jurassic core samples)
Present-day groundwaters (Upper Jurassic)
Celestite-forming waters (Upper Jurassic core samples)
Calcite-forming waters (Middle Jurassic core samples)
Present-day groundwaters (Middle Jurassic)
Calcite-forming waters (Upper and Middle Jurassic outcrop samples)
SMOW
149.2 ± 5.8 Ma
33.2 ± 5.5 Ma
present-day
present-day
δ D / ‰ V-SMOW
Cl⁻ / mmol.l⁻¹
10
0
−10
−20
−30
−40
−50
−60
−70
−80
−90
−100
0.1
1
10
100
1000
10000

Fig. 9

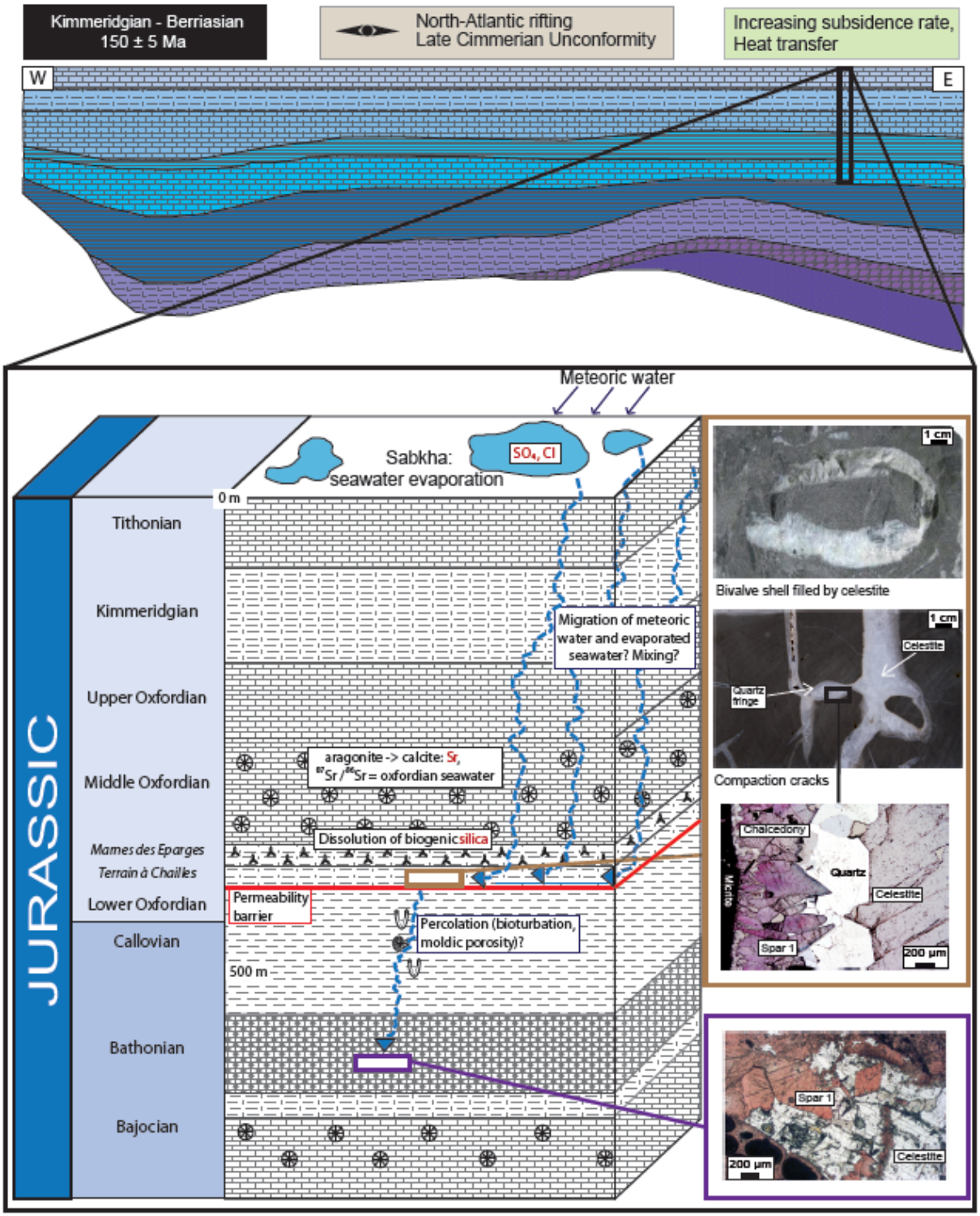
Kimmeridgian - Berriasian
150 ± 5 Ma
North-Atlantic rifting
Late Cimmerian Unconformity
Increasing subsidence rate,
Heat transfer
W
E
Meteoric water
Sabkha:
seawater evaporation
SO4, Cl
0 m
JURASSIC
Tithonian
Kimmeridgian
Upper Oxfordian
Middle Oxfordian
Marnes des Eparges
Terrain à Chailles
Lower Oxfordian
Callovian
Bathonian
Bajocian
Migration of meteoric water and evaporated seawater? Mixing?
aragonite -> calcite: Sr, 87Sr /86Sr = oxfordian seawater
Dissolution of biogenic silica
Permeability barrier
Percolation (bioturbation, moldic porosity)?
500 m
1 cm
Bivalve shell filled by celestite
Celestite
Quartz fringe
Compaction cracks
Chalcedony
Quartz
Celestite
Micrite
Spar 1
200 µm
Spar 1
Celestite
200 µm

Fig. 10

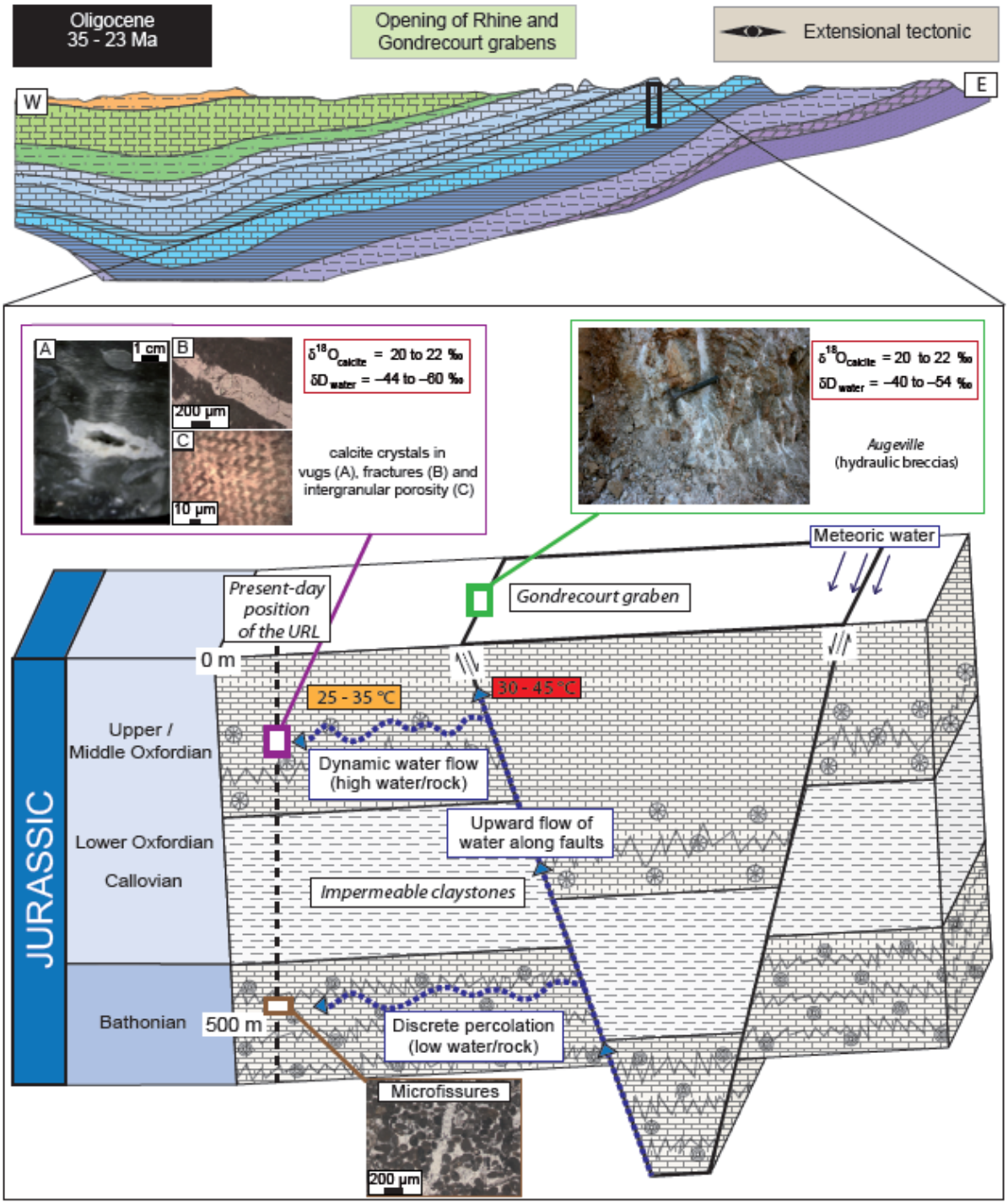
Oligocene
35 - 23 Ma
Opening of Rhine and Gondrecourt grabens
Extensional tectonic
W
E
A
1 cm
B
200 µm
C
10 µm
δ18Ocalcite = 20 to 22 ‰
δDwater = –44 to –60 ‰
calcite crystals in vugs (A), fractures (B) and intergranular porosity (C)
δ18Ocalcite = 20 to 22 ‰
δDwater = –40 to –54 ‰
Augeville
(hydraulic breccias)
Meteoric water
Present-day position of the URL
Gondrecourt graben
0 m
25 - 35 °C
30 - 45 °C
JURASSIC
Upper / Middle Oxfordian
Lower Oxfordian
Callovian
Bathonian
Dynamic water flow (high water/rock)
Upward flow of water along faults
Impermeable claystones
500 m
Discrete percolation (low water/rock)
Microfissures
200 µm

Fig. 11

Table 1

Borehole / Locality	Sample depth - number	Mineral	Stratigraphic position	Sample type	Weight (mg)	H_2O (µmol)	δD (‰ V-SMOW)	$\delta^{18}O_{mineral}$ (‰ V-SMOW)	$\delta^{18}O_{H2O}$ (‰ V-SMOW) T = 35 °C	$\delta^{13}C$ (‰ PDB)	Chlorinity (mmol.l^{-1})
PPA	134 m -1	Calcite	Upper Oxfordian	Vug	3213.2	7.06	–59.5	22.4	–6.4	3.0	0 (5)
PPA	134 m -2	id.	Upper Oxfordian	Vug	8211.9	9.14	–51.7	id.	id.	2.9	id.
HTM102	141 m	id.	Upper Oxfordian	Vug	3589.7	19.10	–48.9	21.4	–7.4	3.1	0 (2)
PPA	184 m -1	id.	Upper Oxfordian	Vug	6211.6	33.41	–44.9	21.7	–7.1	2.7	0 (5)
PPA	184 m -2	id.	Upper Oxfordian	Vug	1846.1	32.87	–44.2	id.	id.	2.8	id.
PAX	324 m -1	Celestite	Middle Oxfordian	Compaction crack	1383.5	5.99	–94.0	19.5	/	/	480 - 3640 (8)
PAX	324 m -2	id.	Middle Oxfordian	Compaction crack	/	/	/	19.8	/	/	id.
PAX	340 m	Calcite	Middle Oxfordian	Vug	3606.8	5.74	–55.6	21.9	–6.9	2.9	0 - 50 (8)
EST413	376 m -1	Celestite	Middle Oxfordian	Moldic porosity	1070	2.12	–94.0	19.4	/	/	1300 - 3660 (8)
EST413	376 m -2	id.	Middle Oxfordian	Moldic porosity	/	/	/	19.1	/	/	id.
PAX	380 m	Quartz	Middle Oxfordian	Compaction crack	1747.2	9.98	/	/	/	/	320 - 3620 (21)
EST433	481 m -1	Calcite	Bathonian	Vug	2225.8	98.05	–20.1	21.3	–7.5	0.0	1000 - 1700 (11)
EST433	481 m -2	id.	Bathonian	Vug	dupl.	dupl.	–20.3	id.	id.	0.5	id.
EST433	569 m -1	id.	Bajocian	Vug	2868.2	117.91	–32.7	24.2	–4.7	2.0	650 - 2700 (10)
EST433	569 m -2	Celestite	Bajocian	Vug	/	/	/	/	/	/	760 - 3840 (7)
EST433	660 m -1	Calcite	Bajocian	Vug	2126.6	25.65	–34.9	24.1	–4.7	2.3	unknown (Fe-calcite)
EST433	660 m -2	id.	Bajocian	Vug	dupl.	dupl.	–35.7	id.	id.	2.7	id.
Augeville	AB71	Calcite	Upper Oxfordian	Hydraulic breccia	2020.7	64.16	–48.1	21.9	–6.9	2.5	0 - 40 (6)
Augeville	AB72	id.	Upper Oxfordian	Hydraulic breccia	1080.8	26.50	–47.6	id.	id.	id.	id.
Augeville	AB7-B1	id.	Upper Oxfordian	Hydraulic breccia	2010.4	18.44	–53.6	id.	id.	id.	id.
Augeville	AB7-B2	id.	Upper Oxfordian	Hydraulic breccia	999.9	9.60	–54.0	id.	id.	id.	id.
Augeville	AB7-C1	id.	Upper Oxfordian	Hydraulic breccia	2011.1	37.73	–45.4	21.7	–7.1	2.0	0 (3)
Augeville	AB7-C2	id.	Upper Oxfordian	Hydraulic breccia	1950.3	39.03	–45.7	id.	id.	id.	id.
Augeville	AB7-GC3	id.	Upper Oxfordian	Hydraulic breccia	1012.0	9.43	–40.8	21.2	–7.6	2.0	0 - 30 (4)
Augeville	AB7-GF1	id.	Upper Oxfordian	Hydraulic breccia	2219.7	123.69	–41.2	20.7	–8.2	1.6	0 (2)
Augeville	AB7-GF2	id.	Upper Oxfordian	Hydraulic breccia	1055.0	43.78	–49.0	id.	id.	id.	id.
Leurville	LEU-3	id.	Upper Oxfordian	Hydraulic breccia	1144.1	15.15	–47.6	21.9	–6.9	1.7	0 - 70 (6)
Leurville	LEU-4	id.	Upper Oxfordian	Hydraulic breccia	2005.3	17.99	–51.9	id.	id.	id.	id.
Sommerécourt	SOM2-1	id.	Bajocian	Vug	2131.4	98.47	–48.4	22.0	–6.8	2.9	0 - 160 (3)
Sommerécourt	SOM2-2	id.	Bajocian	Vug	1005.2	28.46	–51.0	id.	id.	id.	id.

Table 2

borehole	Sample depth	Mineral	Sample type	Stratigraphic position	$\delta^{13}C$ (‰ $_{PDB}$)	$\delta^{18}O_{mineral}$ (‰ $_{V\text{-}SMOW}$)	$\delta^{18}O_{H2O}$ (‰ $_{V\text{-}SMOW}$) T = 35 °C	$^{87}Sr/^{86}Sr$
PAX	380 m	Calcite in host rock (marl)	Vug	Lower Oxfordian	2.1	30.0	1.2	/
id.	id.	Chalcedony	id.	id.	/	32.4	–0.3	/
id.	id.	Quartz	id.	id.	/	33.2	–0.2	/
id.	id.	Calcite spar	id.	id.	1.5	21.2	–7.6	/
id.	324 m	Celestite	Compaction crack	id.	/	/	/	0.706950
PPA	360 m	id.	Compaction crack	Middle Oxfordian	/	/	/	0.707545
id.	372 m	id.	Moldic infilling	Lower Oxfordian	/	/	/	0.706924
EST413	376 m	id.	Moldic infilling	Lower Oxfordian	/	/	/	0.707081
EST433	569 m	Celestite	Vug	Bajocian	/	/	/	0.707140

Highlights

- First data combining δD and chlorinity of fluid inclusions in the Jurassic of the Eastern Paris Basin
- Brines are identified in calcite crystallized at around 150 Ma
- Paleofluid temperatures do not exceed 60 °C
- Independent hydrological history in limestone aquifers on both sides of the Callovian-Oxfordian claystones